Phosphorylation of Gβ is crucial for efficient chemotropism in yeast

Reagan DeFlorio[1,2], Marie-Elena Brett[3,*], Nicholas Waszczak[1,*], Elisabetta Apollinari[1,*], Metodi V. Metodiev[1,‡], Oleksii Dubrovskyi[1,§], David Eddington[3], Robert A. Arkowitz[2] and David E. Stone[1,¶]

[1]Laboratory for Molecular Biology, Department of Biological Sciences, University of Illinois at Chicago, Chicago, IL 60607, USA
[2]CNRS UMR7277/INSERM UMR1091/Université de Nice – Sophia Antipolis, Institute of Biology Valrose, 06108 Nice Cedex 2, France
[3]Department of Bioengineerning, University of Illinois at Chicago, Chicago, IL 60607, USA

*These authors contributed equally to this work
‡Present address: School of Biological Sciences, University of Essex, Essex CO4 3SQ, UK
§Present address: College of Medicine, University of Chicago, Chicago, IL 60637, USA
¶Author for correspondence (dstone@uic.edu)

Accepted 2 April 2013
Journal of Cell Science 126, 2997–3009
© 2013. Published by The Company of Biologists Ltd
doi: 10.1242/jcs.112797

Summary

Mating yeast cells interpret complex pheromone gradients and polarize their growth in the direction of the closest partner. Chemotropic growth depends on both the pheromone receptor and its associated G-protein. Upon activation by the receptor, Gα dissociates from Gβγ and Gβ is subsequently phosphorylated. Free Gβγ signals to the nucleus via a MAPK cascade and recruits Far1–Cdc24 to the incipient growth site. It is not clear how the cell establishes and stabilizes the axis of polarity, but this process is thought to require local signal amplification via the Gβγ–Far1–Cdc24 chemotropic complex, as well as communication between this complex and the activated receptor. Here we show that a mutant form of Gβ that cannot be phosphorylated confers defects in directional sensing and chemotropic growth. Our data suggest that phosphorylation of Gβ plays a role in localized signal amplification and in the dynamic communication between the receptor and the chemotropic complex, which underlie growth site selection and maintenance.

Key words: Gβ phosphorylation, *Saccharomyces cerevisiae*, Chemotropism, Polarized growth, Reorientation, Yeast mating response

Introduction

In metazoans, directed cell movement in response to a chemical gradient (chemotaxis), plays a vital role in embryogenesis, postnatal development and immunity. Moreover, the survival of many single-celled organisms depends on their ability to detect and move in response to chemical stimuli. The related phenomenon, directed cell growth in response to a chemical gradient (chemotropism), is also essential in many species. In mammals, chemotropism is integral to axon guidance (Hong and Nishiyama, 2010; Tojima et al., 2011) and angiogenesis (English et al., 2001; Basile et al., 2004). Pollen tube guidance is also a chemotropic process (Palanivelu and Preuss, 2000; Kim et al., 2004), and there is an increasing appreciation for the role of chemotropism in the life cycles of fungal species, including plant and human pathogens (Snetselaar et al., 1996; Daniels et al., 2006).

Many chemosensing cells express G-protein-coupled receptors (GPCRs) to detect the presence of the extracellular signaling molecules and determine the direction of their source (Weiner, 2002). Using the spatial information encoded in the distribution of activated receptors, the cell establishes a landmark for polarization. Actin and/or microtubule cytoskeletal elements are then assembled at, or recruited to, this site to promote directional movement or growth. Additionally, the cell must be able to stabilize the axis of polarity, while retaining the plasticity to change its orientation in response to changes in the direction of the gradient. Because physiological gradients of chemoattractant are typically very shallow (Mato et al., 1975; Tranquillo et al., 1988; Segall, 1993), establishment of the polarity site requires the conversion of small differences in receptor occupancy into a substantially steeper intracellular signaling gradient. This is thought to depend on feedback loops, such as those first discovered in *Dictyostelium* and neutrophils, that couple local excitation with global inhibition (LEGI) (Iijima et al., 2002; Weiner, 2002; Devreotes and Janetopoulos, 2003).

In comparison to chemotactic models, the amplification mechanisms that underlie directional sensing in chemotropic systems are less well understood. The best-characterized example of eukaryotic chemotropism to date occurs during the mating response of the budding yeast, *Saccharomyces cerevisiae*. In the haploid phase of its life cycle, budding yeast exist as two mating types, *MAT***a** and *MAT*α. Each mating type constitutively secretes a peptide mating pheromone that binds to GPCRs on cells of the opposite type. Liganded receptors activate the mating-specific Gα protein, Gpa1 (henceforth Gα), via guanine nucleotide exchange and the subsequent dissociation of Gα–GTP from the Gβγ dimer, Ste4/Ste18. The signal is then transmitted by Gβγ via the Fus3 MAP kinase (MAPK) cascade that ultimately induces cell-cycle arrest, changes in gene expression and morphogenesis (Dohlman and Thorner, 2001; Bardwell, 2005). Cells polarize their growth and form mating projections, becoming pear-shaped ‘shmoos’, in response to both isotropic pheromone and pheromone gradients. In mating mixtures, cells find and contact the closest potential mating partner by determining the direction of the most potent pheromone source and growing toward it (Jackson and Hartwell, 1990).

Journal of Cell Science

Polarized growth in *S. cerevisiae*, like that in higher eukaryotes, requires the marking of a growth site at the cell cortex and alignment of the actin cytoskeleton towards it. Cargo bound for the polarized structures is transported along the actin cables (Pruyne and Bretscher, 2000a; Pruyne and Bretscher, 2000b). Actin polarization depends on Cdc42, which is thought to activate a formin protein, Bni1, that nucleates and tethers actin cables to the polarization site (Evangelista et al., 2002; Sagot et al., 2002). Bni1 is part of the 'polarisome' complex, together with Spa2, Bud6 and Pea2 (Pruyne and Bretscher, 2000a). Cdc42 is activated by the exchange factor Cdc24, which itself undergoes localized activation during both vegetative budding and mating. In vegetative cells, cortical tags promote localized activation of the monomeric GTPase, Bud1/Rsr1 (hereafter Bud1), which binds directly to Cdc24 (Park et al., 1997) and Cdc42 (Kang et al., 2010). In cells exposed to pheromone, Gβγ interacts with the Far1–Cdc24 complex (Butty et al., 1998; Nern and Arkowitz, 1998; Nern and Arkowitz, 1999). Interaction of Gβγ with Far1 is thought to activate Cdc24 (Wiget et al., 2004), leading to localized GTP-loading of Cdc42, recruitment of Bni1, nucleation of actin cables, and polarized growth, to form the mating projection. The Gβγ–Far1–Cdc24 complex is presumed to assemble in the region of the cell surface that experiences the highest concentration of pheromone and to mark this area for growth in preference to the predetermined bud site (Nern and Arkowitz, 2000). In this way, the cell is thought to orient its growth toward the source of pheromone, although the feedback loops that amplify the directional signal have not been well characterized. When cells are unable to sense a gradient of pheromone, on the other hand, they form a mating projection at the Bud1-marked site that would have been used for the next bud (Dorer et al., 1995; Nern and Arkowitz, 1999). This is called the default mating projection site.

Yeast exhibit a remarkable ability to interpret chemical gradients. It has been estimated that a 1% difference in receptor occupancy across the 5 μm length of a yeast cell in a pheromone gradient is sufficient to elicit robust orientation toward the pheromone source (Segall, 1993), and microfluidic studies suggest an even greater acuity (Moore et al., 2008). How is this very slight asymmetry in activated receptor and G-protein amplified internally to establish a unique shmoo site, and how is this positional information continually communicated to the polarisome to ensure properly oriented growth over time?

Since it was first reported that pheromone induces the phosphorylation of Gβ on multiple sites (Cole and Reed, 1991), the function of this modification has been elusive. A double point mutant form of Gβ that cannot be phosphorylated was found to have no measurable effect on signal transmission, adaptation, or diploid formation (Li et al., 1998). More recently, we discovered that the activated forms of the mating-specific Gα protein and the Fus3 MAPK interact directly. A mutant form of Gα that is severely defective in binding Fus3, $G\alpha^{DSD}$ (Gα-Docking Site Disrupted; previously $G\alpha^{K21E\ R22E}$), confers a defect in partner discrimination, indicating a problem in directional sensing and/or directed growth (Metodiev et al., 2002; Strickfaden and Pryciak, 2008; Yu et al., 2008). $G\alpha^{DSD}$ also results in hypo-phosphorylation and reduced levels of Gβ, as does *fus3*Δ. These observations raised the possibility that the phosphorylation of Gβ plays a role in chemotropism. Here we show that Gβ phosphorylation is critical for this process.

Results

Gα plays an essential role in the chemotropic shmoo pathway

The findings that $G\alpha^{DSD}$ confers partial defects in partner discrimination, mating efficiency, shmooing and actin polarization (Metodiev et al., 2002; Matheos et al., 2004), suggest that the Gα–Fus3 interaction plays a role in chemotropism. Moreover, Gα itself has been implicated in chemotropism (Strickfaden and Pryciak, 2008; Yu et al., 2008). We therefore asked whether $G\alpha^{DSD}$ *bud1*Δ cells can shmoo. Cells can form mating projections if either the default or chemotropic shmoo pathways are inactivated, but are unable to polarize their growth in response to pheromone if neither pathway is functional (Nern and Arkowitz, 2000). Thus, components required for chemotropic growth can be uncovered by examining mutations in a *bud1*Δ background. For example, *cdc24-m1 bud1*Δ and *far1-H7 bud1*Δ cells cannot shmoo (Nern and Arkowitz, 2000) because Cdc24 and Far1 are essential chemotropic elements (Valtz et al., 1995; Nern and Arkowitz, 1998). Similarly, $G\alpha^{DSD}$ *bud1*Δ cells were completely unable to form mating projections (Fig. 1A). Whereas the Gα *bud1Δ* cells and $G\alpha^{DSD}$ *BUD1* cells (not shown) formed normally shaped shmoos, the $G\alpha^{DSD}$ *bud1Δ* cells either enlarged uniformly, or exhibited highly aberrant morphologies, consistent with the idea that the Gα–Fus3 interaction is required for chemotropic growth.

$G\beta^{P-}$ *bud1*Δ cells are defective in shmooing

As Gβ phosphorylation and level are greatly reduced in pheromone-treated $G\alpha^{DSD}$ and *fus3*Δ cells, Gβ may be a target of Gα–Fus3. Because $G\alpha^{DSD}$ also confers defects in partner discrimination and in the genetic assay for 'chemotropic' shmooing described above, we wondered whether the phosphorylation of Gβ plays a role in the chemotropic response. As a first test of this idea, we created strains in which the native *STE4* was replaced with $ste4^{T320A/S335A}$ (Li et al., 1998), which encodes a mutant form of Gβ that is not phosphorylated *in vivo* (henceforth $G\beta^{P-}$), in *BUD1* and *bud1*Δ backgrounds. The $G\beta^{P-}$ *bud1*Δ, Gβ *bud1*Δ, $G\beta^{P-}$ *BUD1* and Gβ *BUD1* (henceforth WT, for wild type) cells were treated with a range of pheromone concentrations and examined over 5 hours. In isotropic pheromone, $G\beta^{P-}$ *BUD1* cells were indistinguishable from WT cells. In contrast, $G\beta^{P-}$ *bud1*Δ cells exhibited a variety of shmoo abnormalities at all doses and time points. Representative images are shown in Fig. 1B.

A high proportion of the $G\beta^{P-}$ *bud1*Δ shmoos were shorter and broader than those formed by the Gβ *bud1*Δ control cells, as if their growth was less well focused. Their mean lengths were 0.89 and 0.84 that of the Gβ *bud1*Δ cells 4 and 5 hours after treatment, respectively ($P<0.0001$; $n=300$ for each time point), and most were abnormally shaped. Instead of narrowing smoothly to a pointed tip, $G\beta^{P-}$ *bud1*Δ mating projections often extended almost straight out from the cell body and terminated in a bulbous curve. Although aberrant shmoo morphologies were also seen in the Gβ *bud1*Δ culture, likely due to the absence of Bud1, their occurrence was greatly increased by $G\beta^{P-}$ (80.7% as compared to 16.7%; $n\geq260$; $P<0.0001$).

Wild-type cells treated with high pheromone concentrations form successive mating projections with regular periodicity such that the growth of the first projection ends as the second begins (Bidlingmaier and Snyder, 2004). In isotropic pheromone, the second growth site is usually established far from the first one, so

Journal of Cell Science

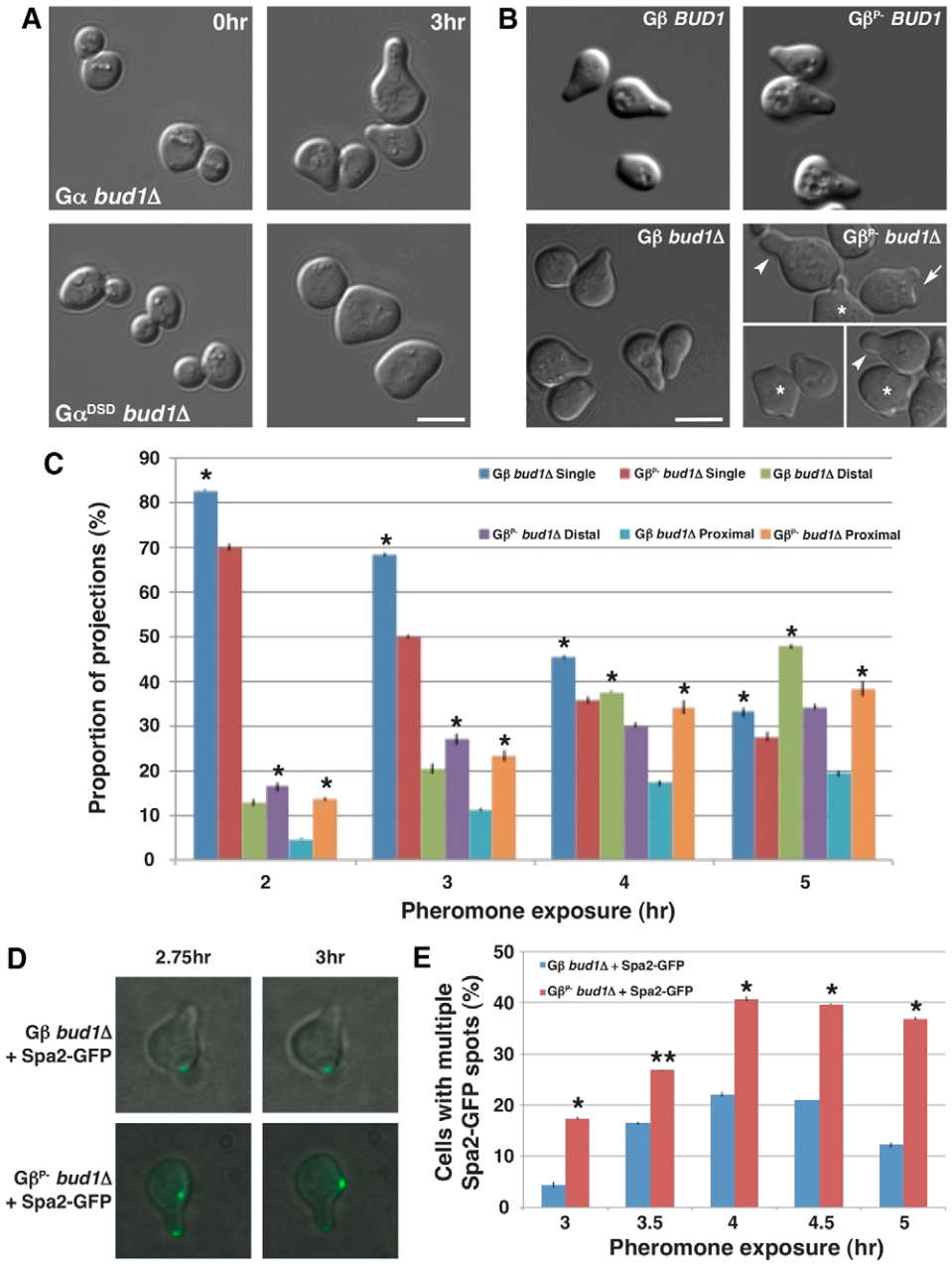

Fig. 1. Effect of $G\alpha^{DSD}$ and $G\beta^{P-}$ on the chemotropic shmoo pathway. (**A**) $G\alpha^{DSD}$ *bud1*Δ cells are unable to form mating projections. *MAT***a** *gpa1*Δ *bud1*Δ cells expressing either Gα or $G\alpha^{DSD}$ were exposed to 150 nM pheromone for 3 hours. (**B**) $G\beta^{P-}$ *bud1*Δ cells exhibit a variety of mating projection abnormalities. *MAT***a** Gβ *bud1*Δ, $G\beta^{P-}$ *bud1*Δ, Gβ *BUD1* and $G\beta^{P-}$ *BUD1* cells were exposed to 30 nM pheromone for 3 hours. Representative images are shown. Lower right image is a composite. White arrowheads indicate cells scored as bulbous shmoos; white arrows indicate proximal double shmoos; and white asterisks mark SMP cells. (**C**) $G\beta^{P-}$ *bud1*Δ cells form projections proximal to the initial growth site. *MAT***a** Gβ *bud1*Δ and $G\beta^{P-}$ *bud1*Δ cells were exposed to 30 nM pheromone and the percentages of cells with a single projection, multiple distal projections, and multiple proximal projections were determined at each time point. The means ± s.e.m. of three independent experiments are shown ($n \geq 200$ for each strain and time). *$P<0.0001$ comparing the higher and lower percentages of a given projection type. (**D**) Simultaneous localization of Spa2–GFP to multiple projection tips. *MAT***a** Gβ *bud1*Δ and $G\beta^{P-}$ *bud1*Δ cells expressing *SPA2-GFP* were exposed to 150 nM pheromone for 3 hours. Representative images are shown. (**E**) Percentage of cells showing simultaneous localization of Spa2–GFP to multiple projection tips. The means ± s.e.m. of three independent experiments are shown ($n>120$ for each strain and time); *$P<0.0001$, **$P<0.005$. Scale bars: 5 μm.

that the two projections ultimately form a wide angle (distal projections). Another striking phenotype of the $G\beta^{P-}$ *bud1*Δ cells was their tendency to form second and third mating projections earlier than the control cells and in abnormal positions (Fig. 1C). In the control strain, we observed a small fraction of cells with two or more projections adjacent to one another (proximal projections). However, the occurrence of such cells was dramatically increased in the $G\beta^{P-}$ *bud1*Δ strain, with the ratio of proximal to distal shmoos more than 10-fold greater in $G\beta^{P-}$ as compared to control cells. Similar results were observed at all pheromone concentrations and incubation times. Interestingly, the Spa2–GFP marker of polarized growth simultaneously localized to more than one shmoo tip in a high proportion of $G\beta^{P-}$ *bud1*Δ cells (Fig. 1D), suggesting that Gβ phosphorylation is involved in switching growth from one site to another.

Although $G\beta^{P-}$ *bud1*Δ cells were not completely incapable of polarized growth in isotropic pheromone, as are $G\alpha^{DSD}$ *bud1*Δ and *cdc24-m*1 *bud1*Δ cells, a significant fraction were unable to sustain unidirectional growth long enough to form a projection. Such cells were usually quite small, and formed multiple protrusions unlike true mating projections. In Fig. 1C, these cells are counted in the 'multiple proximal' category; we refer to them as small multiple protrusion (SMP) cells. [The SMP percentages (mean ± s.e.m.) were 16.2±1.4 and 4.0±0.5 for the $G\beta^{P-}$ *bud1*Δ and Gβ *bud1*Δ cultures, respectively; $n \geq 200$; $P<0.0001$.] Together, the results presented in Fig. 1B–D suggest that, in cells unable to shmoo via the Bud1-dependent default pathway, Gβ phosphorylation is critical for stabilization of the axis of polarity (hence for focused growth of the mating projection) and for proper growth-site switching.

The growth site of pheromone-treated Gβ^{P-} *bud1*Δ cells wanders where the receptor is concentrated

Nern and Arkowitz (Nern and Arkowitz, 2000) found that double mutants lacking both the default and chemotropic pathways are unable to shmoo because they cannot stabilize their axis of polarity long enough to polarize their growth, not because they cannot establish polarity. The recent demonstration that the Bem1–GFP polarity marker wanders rapidly around the membrane of pheromone-treated *cdc24-m1 bud1*Δ cells (Dyer et al., 2013) supports this conclusion. Could the blunt shmoo and SMP phenotypes be the result of a less severe wandering-axis phenotype? To test this, we mixed *MAT***a** Gβ^{P-} *bud1*Δ and *MAT***a** Gβ *bud1*Δ cells expressing Spa2–GFP with WT *MAT*α cells, and assayed reporter localization over time (Fig. 2A). In the control cells, Spa2–GFP localized tightly to the tip of the growing mating projection, moving steadily outward along the axis of polarity. In

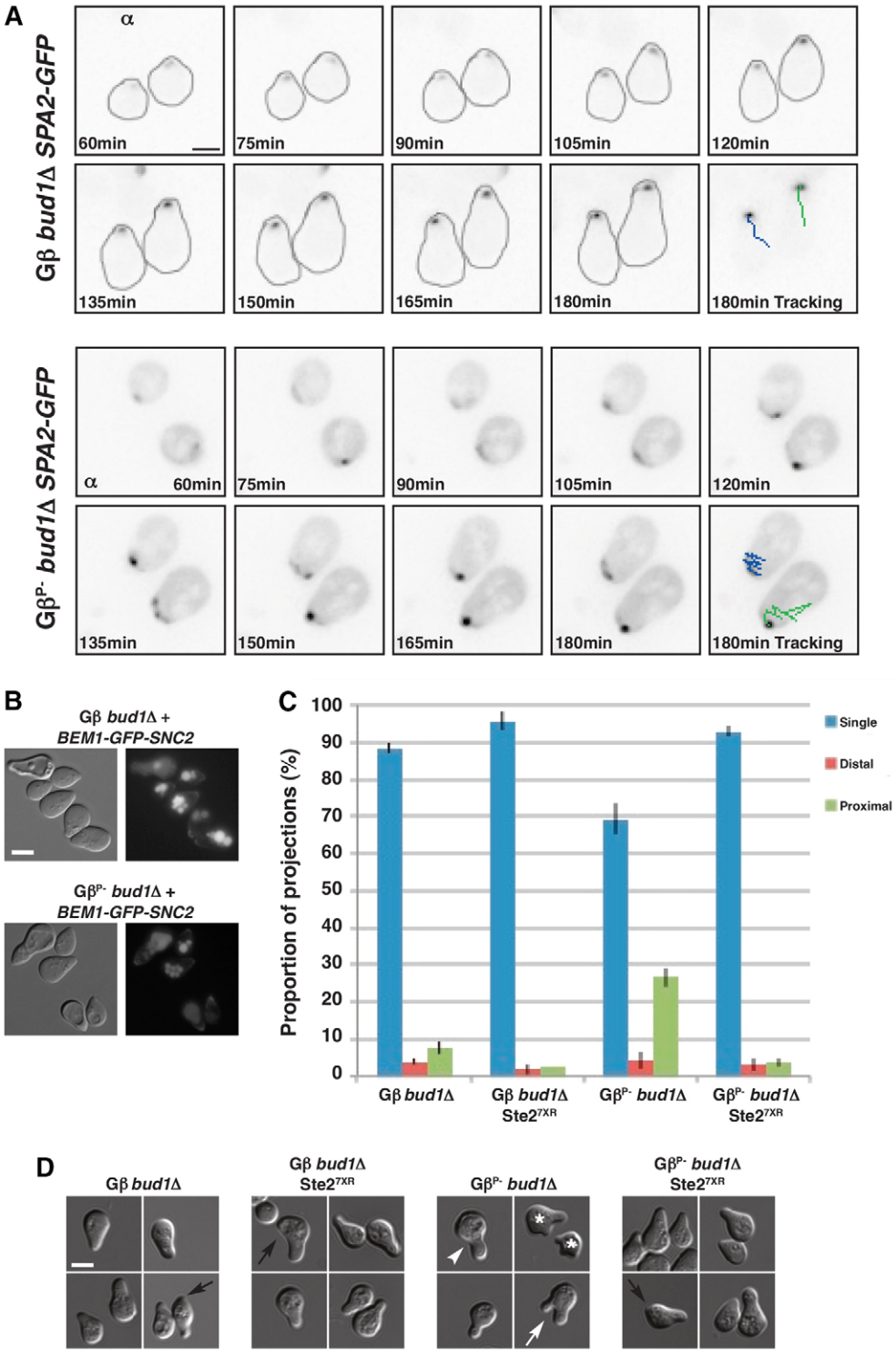

Fig. 2. The growth site of pheromone-treated Gβ^{P-} *bud1*Δ cells wanders where the receptor is concentrated. (**A**) Time-lapse images of Spa2–GFP in mating cells. *MAT***a** Gβ *bud1*Δ or Gβ^{P-} *bud1*Δ cells expressing *SPA2-GFP* were mixed with *MAT*α cells and incubated for the indicated times. Final images show an overlay of Spa2–GFP movement from 60–180 minutes; α indicates the position of the closest *MAT*α cell at 60 minutes. (**B**) Bem1–GFP–Snc2 rescues the Gβ^{P-} *bud1*Δ shmoo abnormalities. *MAT***a** Gβ *bud1*Δ or Gβ^{P-} *bud1*Δ cells expressing *BEM1-GFP-SNC2* were exposed to 30 nM pheromone for 3 hours. Representative DIC and fluorescent images are shown. (**C**) Gβ^{P-} *bud1*Δ cells do not form proximal projections when receptor internalization is blocked. *MAT***a** Gβ *bud1*Δ, Gβ *bud1*Δ *ste2*$^{7XR/GPAAD}$, Gβ^{P-} *bud1*Δ and Gβ^{P-} *bud1*Δ *ste2*$^{7XR/GPAAD}$ cells were exposed to 25 nM pheromone for 4 hours. The percentages of cells with a single projection, multiple distal projections and multiple proximal projections were determined. The means±s.e.m. of three independent experiments are shown (n=300 for each strain and trial). P<0.0001 for the % single projections and % proximal projections formed by the Gβ^{P-} *bud1*Δ strain as compared with the other three strains. (**D**) Representative images from the experiment quantified in C. White arrowheads indicate single shmoos; black arrows indicate distal double shmoos; white arrows indicate proximal double shmoos; and white asterisks mark SMP cells (which are counted in the proximal shmoo category). Scale bars: 5 μm.

Journal of Cell Science

$G\beta^{P-}$ *bud1*Δ cells, Spa2–GFP moved more than twice as far, even though the mutant shmoos elongated at the same rate as the control cells. The increased mobility of Spa2–GFP correlated with an increased tendency to change direction (Table 1). Multiple Spa2–GFP spots were also commonly observed in the mutant, but rarely in control cells. Thus, the axis of polarity exhibited confined wandering within the broad mating projections formed by $G\beta^{P-}$ *bud1*Δ cells during mating.

Essential regulators of actin cable polymerization (e.g. Cdc24–Cdc42, Bem1, Spa2) cluster tightly in a patch at the tips of shmooing cells (Pruyne and Bretscher, 2000a; Arkowitz, 2009). In pheromone-treated WT cells, this 'polarity patch' wanders along the cell cortex, becoming restricted in its movement around the incipient growth site (Dyer et al., 2013). Polarity patch movement is thought to be retarded by free Gβγ, whose concentration is ultimately determined by the local density of activated receptor. The role of the receptor and Gβγ in stabilizing the polarity patch can be bypassed by a chimeric protein consisting of Bem1 and the transmembrane domain of Snc2. Expression of Bem1–GFP–Snc2 dramatically slowed movement of the polarity patch, focusing the growth of WT cells and restoring the ability of *cdc24-m1 bud1*Δ cells to shmoo (Dyer et al., 2013). If the shmoo morphology and maintenance defects displayed by $G\beta^{P-}$ *bud1*Δ cells are also due to a wandering axis of polarity stemming from a weakened link between the receptor and polarity patch, we would expect these phenotypes to be suppressed by Bem1–GFP–Snc2 as well. This proved to be the case: The shmoos formed by Gβ *bud1*Δ and $G\beta^{P-}$ *bud1*Δ cells transformed with the Bem1–GFP–Snc2 construct were indistinguishable (Fig. 2B).

Pheromone triggers polarization of the receptor and G-protein to the mating projection (Suchkov et al., 2010) – the same area where the growth site wanders in $G\beta^{P-}$ *bud1Δ* cells. This confined wandering might underlie the formation of proximal projections. To determine whether receptor polarity influences the tendency of $G\beta^{P-}$ *bud1*Δ cells to form proximal mating projections, we constructed $G\beta^{P-}$ *bud1*Δ and Gβ *bud1*Δ strains expressing the $Ste2^{7XR/GPAAD}$ mutant form of the receptor. $Ste2^{7XR/GPAAD}$ cannot be internalized (Ballon et al., 2006) and therefore does not polarize in response to pheromone (Suchkov et al., 2010). Although cells expressing $Ste2^{7XR/GPAAD}$ also formed blunt shmoos, preventing receptor polarization suppressed the formation of proximal projections by $G\beta^{P-}$ *bud1*Δ cells (Fig. 2C), consistent with our hypothesis.

Together, the data shown in Fig. 2 indicate that, although the axis of polarity wanders in $G\beta^{P-}$ *bud1*Δ cells, the movement of the growth site is limited to the region of highest receptor density. This implies that Gβ phosphorylation helps link the position of the polarity proteins to that of the receptor.

Effect of Gβ phosphorylation on Gβ localization

The phenotypes we observe in $G\beta^{P-}$ *bud1*Δ cells could result from improper localization of the mutant Gβ. To test this, we tagged the N-termini of WT Gβ and $G\beta^{P-}$ with GFP *in situ*. In isotropic pheromone, GFP–$G\beta^{P-}$ polarized to the incipient shmoo site later and less stably than did GFP–Gβ. Similar but more pronounced defects were observed in mating mixtures (Table 2; Fig. 3). Notably, a substantial fraction of mating GFP–Gβ cells switched from one polarization site to another, presumably to align with the strongest ambient gradient. In contrast, mating GFP–$G\beta^{P-}$ cells were defective in site switching, as well as in consolidating Gβ in a single region of the membrane. These data suggest that Gβ phosphorylation plays an important role in the pheromone-induced redistribution of Gβ, particularly in gradient-stimulated cells.

Effects of $G\beta^{P-}$ on Gβ–Far1 interaction and Spa2 and Cdc42 dynamics

The inability to phosphorylate Gβ could also impact the cell by affecting the strength of Gβ interactions. For example, Ste5 preferentially binds the phosphorylated form of Gβ in yeast (Feng et al., 1998), and phosphorylation affects the activity of a mammalian Gβ (Chakrabarti and Gintzler, 2003). Given the phenotypes conferred by $G\beta^{P-}$, the interaction of Gβ with the Far1–Cdc24 chemotropic complex is a good candidate to be regulated by Gβ phosphorylation. To test this, we used a well-established genetic assay (Whiteway et al., 1990; Cole et al., 1990; Bar et al., 2003; Draper et al., 2009) to ask whether Far1 can discriminate between Gβ and $G\beta^{P-}$. The assay is based on the observation that by triggering the pheromone-responsive MAPK pathway, Gβ overexpression blocks cell-cycle progression. Co-overexpression of a protein that binds Gβ can prevent pathway induction and thereby rescue the vegetative growth of cells expressing excess Gβ. At the level of transcriptional induction, cell-cycle arrest and shmooing, Gβ and $G\beta^{P-}$ appear to be equally potent (Li et al., 1998). Nevertheless, Far1 overexpression specifically rescued the cell growth defect due to the overexpression of $G\beta^{P-}$, and not that of Gβ (supplementary material Fig. S1), suggesting that Far1 has a greater affinity for the unphosphorylated form of Gβ.

As a complementary way of assaying the effect of Gβ phosphorylation on Gβγ–Far1 interaction, we performed pull-down assays. Cells overexpressing His-tagged Gγ and either Gβ or $G\beta^{P-}$ were treated with pheromone to induce phosphorylation of WT Gβ before purifying Gβγ and $G\beta^{P-}$ γ on nickel beads. Because Far1 is a low-level protein (Ghaemmaghami et al., 2003), we used mass spectrometric analysis rather than western blotting to measure the amount of co-purifying Far1. Consistent with the results of the genetic assay, Far1 was detectable on the $G\beta^{P-}$ γ but not on the Gβγ beads (supplementary material Fig. S2).

Table 1. Spa2–GFP mobility

Strain	Movement/15 minutes (μm)[a]	Velocity (μm/hour)[a]	ΔDirection (%)[a,b]	Final length (μm)[c]	≥2 spots[a,d]	*n*
$G\beta^{WT}$ *bud1*Δ	0.54±0.15	2.15±0.61	19±13	8.07±0.97	1	89
$G\beta^{P-}$ *bud1*Δ	1.13±0.24	4.51±0.96	52±15	7.39±1.10	18	38

[a]$P<0.0001$.
[b]ΔDirection (%) is the number of direction changes divided by the number of steps observed for each cell.
[c]$P<0.0007$.
[d]Number of Gβ-polarized cells in which the region of concentrated Gβ was composed of two or more discreet spots.

Table 2. Pheromone-induced polarization of Gβ

	Isotropic			Mating		
Parameter	GFP–Gβ	GFP–Gβ^{P-}	*P*-value	GFP–Gβ	GFP–Gβ^{P-}	*P*-value
Polarized *n*/total *n*	47/49	39/52	–	33/36	25/43	–
% Polarized Gβ	95.9	75	<0.0001	91.7	58.1	<0.0001
Mean time of Gβ polarization (minutes)[a]	1. 8±0.4	17.3±1.73	<0.0001	−8.8±2.4	16.8±4.2	<0.0001
% Polarized Gβ pre-polarized growth[b]	55.3	38.4	0.034	84.8	28.0	0.0001
% Switch[c]	NA	NA	–	39.4	12.0	0.005
% Wandering[d]	ND	ND	–	9.1	36.0	0.0001
% Not consolidated[e]	ND	ND	–	34.4	92.0	<0.0001
% Spots[f]	ND	ND	–	21.2	72.0	<0.0001

[a]For the cells that polarized Gβ, the mean±s.e.m. of times of polarization relative to the onset of polarized growth are indicated.
[b]Percentage of Gβ-polarized cells in which polarization occurred at or before morphogenesis.
[c]Percentage of Gβ-polarized cells that clearly switched polarization sites during the time-course.
[d]Percentage of Gβ-polarized cells in which the region of concentrated Gβ appeared to wander.
[e]Percentage of Gβ-polarized cells in which the region of concentrated Gβ was composed of two or more discreet spots.
[f]Percentage of Gβ-polarized cells in which high-intensity spots were observed well apart from the region of concentrated Gβ.
NA, not applicable; ND, not detectable.

To further investigate the possibility that Gβ phosphorylation affects the dynamic interactions of the chemotropic complex, we used fluorescence photobleaching approaches. First, we compared recovery times of the Spa2–GFP signal after photobleaching the shmoo tips of Gβ^{P-} *bud1*Δ and Gβ *bud1*Δ cells. As a component of the polarisome, the positional stability of Spa2 is likely linked to that of the chemotropic complex. In FRAP analysis, the recovery time is a function of the protein's dynamics: The slower the exchange into and out of a complex, the longer the signal will take to recover. As shown in Fig. 4A, the signal recovered in bleached Gβ *bud1*Δ shmoo tips faster and to a greater degree than in bleached Gβ^{P-} *bud1*Δ shmoo tips. This suggests that the duration of Spa2 interactions at the shmoo tip is increased when Gβ cannot be phosphorylated.

To assess the effect of Gβ^{P-} on the stability of the chemotropic complex itself, we performed iFRAP analysis of GFP–Cdc42 at the shmoo tips of Gβ^{P-} *bud1*Δ and Gβ *bud1*Δ cells. In this technique, the area that serves as a source of molecules bound for the complex of interest is photobleached, and the rate at which the signal intensity decreases at the site of complex formation is measured. The rate of signal loss is inversely related to the stability of the complex. In our experiment, the rate of GFP–Cdc42 signal loss at the shmoo tip was determined after bleaching the cell body. As shown in Fig. 4C, the Cdc42–GFP signal decreased faster in Gβ *bud1*Δ than in the Gβ^{P-} *bud1*Δ shmoo tips. Consistent with the Spa2–GFP FRAP results, this suggests that the duration of Cdc42 interactions at the shmoo tip are increased when Gβ cannot be phosphorylated. Together, these data suggest that unphosphorylated Gβ binds more tightly than phosphorylated Gβ to components of the chemotropic complex and/or polarisome. Thus, Gβ phosphorylation may negatively affect the stability of the chemotropic complex and/or polarisome.

Gβ^{P-} confers a defect in chemotropism

In *bud1*Δ cells, mating projection formation depends on chemotropic components (Nern and Arkowitz, 2000). Therefore, the observation that Gβ^{P-} *bud1*Δ cells shmoo aberrantly in isotropic pheromone implicates Gβ phosphorylation in chemotropism. To test this, we set up dilute bilateral mating mixtures in which the cells best able to form stable, chemotropic mating projections were most likely to find and fuse with a partner, and analyzed images of newly formed zygotes (Fig. 5A). How precisely a cell orients towards a potential partner can be inferred by measuring the angle created when two cells fuse. When orientation is optimal, the two cells of a mating pair grow directly toward one another, and consequently, their angle of fusion is ~0°. In contrast, large fusion angles are indicative of poor orientation. In the zygote formation assay, Gβ^{P-} cells exhibited a clear orientation defect (Fig. 5C).

After initial orientation toward a pheromone source, yeast can alter their growth in response to a directional change in the gradient (Segall, 1993; Moore et al., 2008) – either by initiating a second projection, or by bending the existing projection toward the new source (Moore et al., 2008). These phenomena are collectively referred to as *reorientation*. The mechanisms underlying reorientation are likely to overlap and/or interact with those involved in orientation and maintenance. As our data implicate Gβ phosphorylation in initial orientation and stable chemotropic growth, we asked whether it is involved in reorientation as well. WT and Gβ^{P-} bilateral mating mixtures were shaken vigorously to induce non-directional (default) shmooing while preventing cell fusion, then allowed to produce and respond to pheromone gradients on solid medium. Gβ^{P-} conferred a reorientation defect (Fig. 5B,C). Whereas pre-stimulated WT cells often bent dramatically to contact a mating partner, Gβ^{P-} cells formed zygotes that were predominantly the result of 'collision matings', i.e. two shmoos appeared to have simply grown into one another without having significantly changed their direction of growth.

One explanation for the results of the orientation and reorientation assays is that Gβ^{P-} confers a defect in directional sensing and/or chemotropic shmooing. However, it is also possible that Gβ^{P-} cells signal their positions less effectively than WT cells because their pheromone secretion is less focused. We distinguished these possibilities by comparing the ability of Gβ and Gβ^{P-} cells to grow toward a pheromone source *in vitro*, using a microfluidic device (Brett et al., 2012). As previously reported, the Gβ control cells formed normal mating projections in the artificial gradient (Fig. 6A) and oriented toward its source with an accuracy similar to that observed in other published microfluidic experiments (Brett et al., 2012). Surprisingly, the Gβ^{P-} cells were unable to sustain growth in a single direction. Rather, they formed multiple small protrusions, often without growing much in overall size – very much like the SMP cells in

Journal of Cell Science

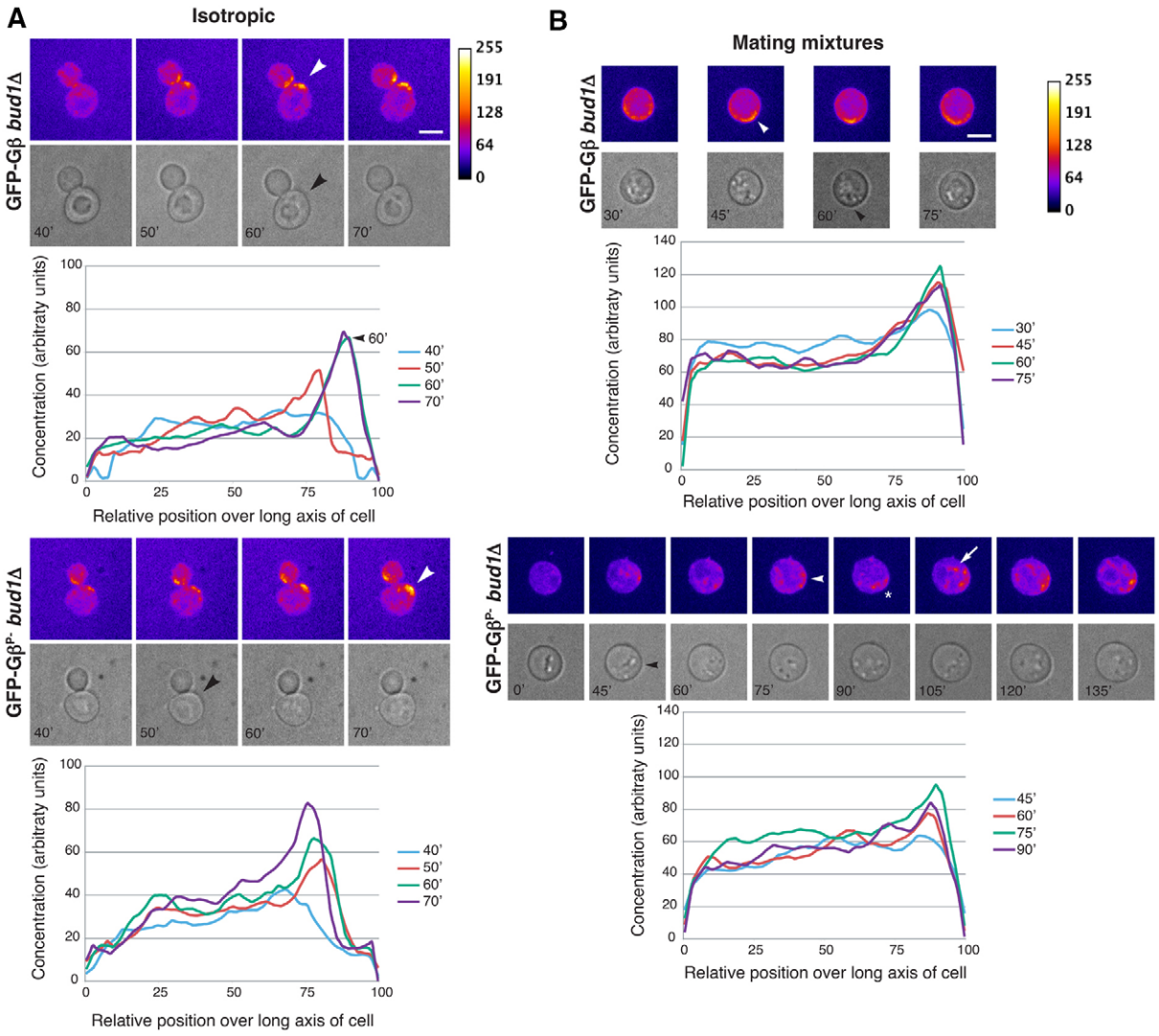

Fig. 3. GFP–Gβ^{P-} polarizes later and less stably than GFP–Gβ in both isotropic and gradient conditions. (**A**) Isotropic treatment: *MAT***a** GFP–Gβ *bud1*Δ and GFP–Gβ^{P-} *bud1*Δ cells were exposed to 150 nM pheromone for the indicated times. (**B**) Mating mixtures: *MAT***a** GFP–Gβ *bud1*Δ and GFP–Gβ^{P-} *bud1*Δ cells were mixed with *MAT*α cells, and incubated for the indicated times. For A and B, GFP–Gβ concentration in arbitrary units was quantified along the major axis of each cell (line graphs) as described in the Materials and Methods; black arrowheads mark polarized growth and white arrowheads mark polarity. For B, white arrows mark spots and the white asterisk marks non-consolidated polarization. The Gβ polarization data are summarized in Table 2. Scale bars: 5 μm.

Gβ^{P} *bud1*Δ cultures treated with isotropic pheromone (Fig. 1B). The first protrusions formed by the gradient-stimulated Gβ^{P-} cells were positioned randomly. These data strongly support the idea that Gβ phosphorylation plays a role in the positioning and maintenance of the chemotropic growth site.

The inability of Gβ^{P-} cells to maintain a single axis of polarity in an artificial gradient, combined with their ability to form normal mating projections in isotropic pheromone, provides the first example, to our knowledge, of a gradient-specific shmoo phenotype. We therefore wished to confirm this observation using natural gradients. To look for gradient-dependent destabilization of polarized growth under physiological conditions, we compared WT and Gβ^{P-} shmoos formed in liquid culture (isotropic treatment) with those formed in bilateral crosses. Although the Gβ^{P-} cells in mating mixtures were not as severely compromised in chemotropic shmooing as the Gβ^{P-} cells in the microfluidic device, they exhibited a number of obvious shmoo defects (Fig. 6B,C). In fact, the response of Gβ^{P-} *BUD1* cells exposed to natural pheromone gradients was the same as that of Gβ^{P-} *bud1*Δ cells exposed to isotropic pheromone: Gβ^{P-} mating mixtures accumulated fewer shmoos, shorter shmoos (their mean length was 0.852 of the control cells after 5 hours of mating; $n \geq 105$; $P < 0.0001$), and a significantly higher proportion of aberrant shmoos. In contrast, the Gβ^{P-} and WT shmoos induced by isotropic treatment were indistinguishable at all concentrations and time points (Fig. 1B). These data suggest that the phosphorylation of Gβ plays a critical role in chemotropic, but not default, shmooing.

Discussion

The rapid phosphorylation of Gβ in yeast cells responding to mating pheromone was observed over 20 years ago (Cole and Reed, 1991), and yet its purpose has remained enigmatic. Two early studies failed

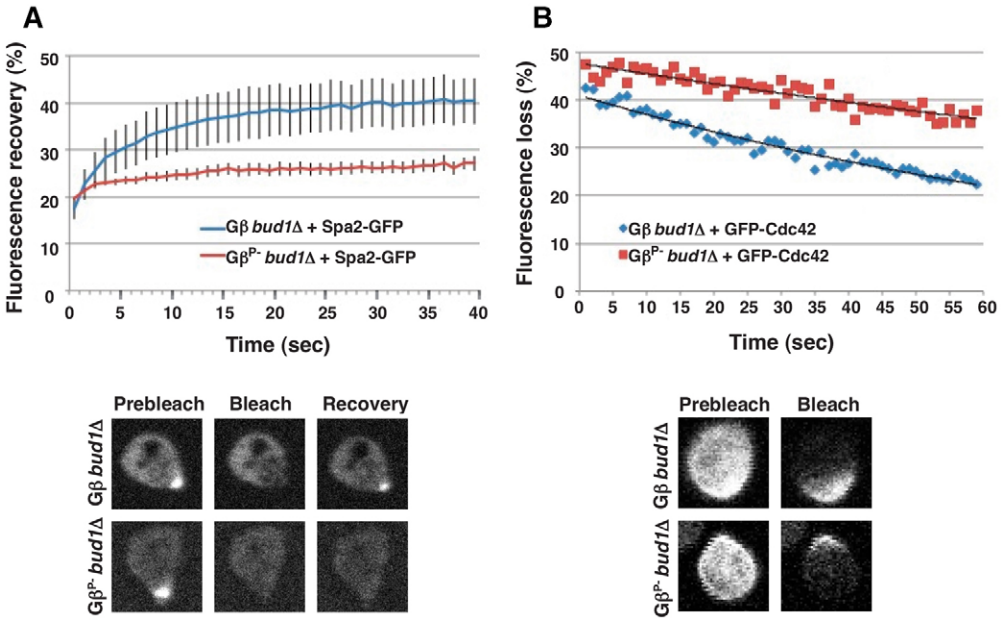

Fig. 4. Effect of $G\beta^{P-}$ on positional stability of Spa2 and Cdc42. (**A**) FRAP analysis of Spa2-GFP. *MAT***a** Gβ *bud1*Δ and $G\beta^{P-}$ *bud1*Δ cells expressing *SPA2-GFP* were exposed to 30 nM pheromone for 1 hour prior to photobleaching. The data represent the means±s.e.m. of two independent experiments. The FRAP $t_{1/2}$ and % recovery were 9.7±1.87 seconds and 40.3±3.43%, respectively, in Gβ *bud1*Δ cells (n=18) and 19.3±2.32 seconds (P=0.003) and 24.6±1.73% (P=0.0002) in $G\beta^{P-}$ *bud1*Δ cells (n=20). Images are shown from a representative FRAP experiment before, subsequent to photobleaching and after 26 seconds recovery. (**B**) iFRAP analysis of GFP–Cdc42. *MAT***a** Gβ *bud1*Δ and $G\beta^{P-}$ *bud1*Δ cells expressing *GFP-CDC42* were exposed to pheromone as above. Representative scatter plots of fluorescence loss and corresponding trend lines are shown. The iFRAP $t_{1/2}$ and % loss were 41.9±3.25 seconds and 22.9±1.48%, respectively, in Gβ *bud1*Δ cells (n=27), and 54.3±3.55 seconds (P=0.01) and 21.1±3.05% in $G\beta^{P-}$ *bud1*Δ cells (n=28). Images are shown from a representative iFRAP experiment before and subsequent to photobleaching.

to elucidate its role (Cole and Reed, 1991; Li et al., 1998). We were impelled to revisit this issue by the discovery that the activated forms of Gα and Fus3 interact, and that a double mutation that uncouples them, $G\alpha^{DSD}$, conferred defects in mating and partner discrimination (Metodiev et al., 2002). Indeed, we show here that $G\alpha^{DSD}$ *bud1*Δ cells cannot form mating projections, which identifies $G\alpha^{DSD}$ as a chemotropic-defective allele (Fig. 1A). This suggests that the Gα–Fus3 interaction, like the Cdc24–Far1 interaction, is critical for chemotropism. Because $G\alpha^{DSD}$ also results in reduced Gβ phosphorylation and protein levels in stimulated cells, we hypothesized that Gβ phosphorylation plays a role in chemotropism. Our results demonstrate that this is the case. Specifically, the modification of Gβ appears to promote communication between activated receptors and downstream components essential for polarized growth. Cells unable to phosphorylate Gβ exhibit defects in pheromone-induced morphogenesis, and both orientation and reorientation towards mating partners. We propose that Gβ phosphorylation provides a means to amplify the spatial signal and that the Gβ phosphorylation/dephosphorylation cycle is an updating mechanism that conveys the status of the receptor to the chemotropic complex.

Aberrant shmoo morphology and proximal projections: wandering limited by high receptor and Gβγ density

Although not completely unable to form mating projections, $G\beta^{P-}$ *bud1*Δ cells exhibited a variety of shmoo abnormalities (Fig. 1B,C), including short and blunt shmoos, cells that formed multiple projections proximal to the first, and very small cells with multiple protrusions (SMP cells). Time-lapse imaging of Spa2–GFP in these cells indicated that the axis of polarity wandered, albeit in a confined area (Fig. 2A). This broader movement of Spa2 correlated with the generation of proximal projections in the region expected to be highest in receptor density. It is therefore of significance that preventing receptor polarization in $G\beta^{P-}$ *bud1*Δ cells dramatically suppressed the proximal-projection phenotype, and that expression of Bem1–GFP–Snc2, which slows polarity site wandering by a mechanism independent of the receptor and G-protein, restored their ability to shmoo normally (Fig. 2B,C). These observations suggest that although the axis of polarity is destabilized in pheromone-treated $G\beta^{P-}$ *bud1*Δ cells, its wandering is limited by the high concentration of receptor and Gβγ in mating projections. This confined wandering likely underlies the formation of short, blunt shmoos, and in combination with the apparent defect in regulating growth-site switching (Fig. 1D; Table 2), may result in the emergence of multiple projections proximal to the first. The occurrence of ≥2 Spa2–GFP spots in $G\beta^{P-}$ *bud1*Δ shmoos also correlates with the eventual formation of proximal projections (Table 1).

Role of Gβ phosphorylation in receptor communication to actin cables

What causes confined wandering? Yeast chemotropism requires the translation of an extracellular pheromone gradient into a gradient of activated receptors across the cell surface, and the communication of this spatial information to the actin cytoskeleton. The receptor does not communicate with actin directly, but rather via its Gβγ, which recruits Far1–Cdc24.

Journal of Cell Science

Journal of Cell Science

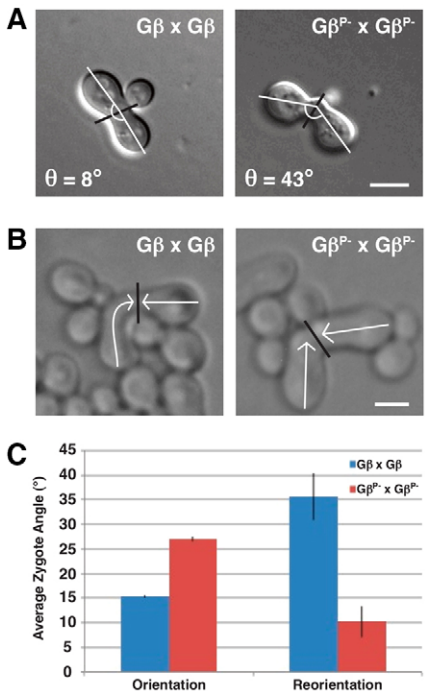

Fig. 5. Gβ^{P-} confers a defect in directional sensing. (**A**) Representative straight and angled zygotes from the orientation assays. Zygotes were analyzed from WT and Gβ^{P-} bilateral matings. The angle of orientation was measured by drawing a line from the base of each shmooing cell (white) to the zone of fusion (black). (**B**) Representative zygotes from the reorientation assays. Pre-stimulated *MAT***a** and *MAT*α cells were allowed to mate on agar media and scored for their ability to reorient growth of an existing mating projection. Zygotes were analyzed from WT and *MAT***a** Gβ^{P-} bilateral matings. Reorientation was defined as a change in direction in a line drawn from the base of a shmoo to the zone of fusion. The angle of reorientation for a given shmoo was measured by drawing a line from the original axis of polarity (white) to the zone of fusion (black). (**C**) Mean ± s.e.m. of the angles of orientation and reorientation. For orientation, $n>200$ for each strain in three trials; $P<0.0001$. For reorientation, $n=58$ for both strains; $P<0.0001$. Scale bars: 5 µm.

Along with the polarisome, Cdc42 and Bem1, the Gβγ–Far1–Cdc24 chemotropic complex ultimately nucleates actin cables at the incipient mating projection site. In *cdc24-m1* and *far1-H7* cells, the link between the receptor and chemotropic complex is completely severed. Polarization sites are established in such cells (Nern and Arkowitz, 2000), but they lack the constraint provided by interaction with receptor-activated Gβγ (Dyer et al., 2013). Hence, their position is not sufficiently stable to sustain polarized growth in one direction. Gβ^{P-} *bud1*Δ cells exhibit a similar, although less severe, phenotype. Instead of global wandering and uniform growth, wandering is confined to the area of most concentrated receptor. This implies that the link between the receptor and chemotropic complex is weakened, but not broken.

We explored the effect of Gβ phosphorylation on the stability of the chemotropic complex and polarisome. A genetic assay suggested that phosphorylation of Gβ reduces its affinity for Far1 (supplementary material Fig. S1), which was supported by the results of a Gβγ pull-down experiment (supplementary material Fig. S2). Photobleaching approaches indicated that both Spa2 and Cdc42 are more mobile in WT cells than in Gβ^{P-} cells, consistent with shorter-lived associations at shmoo tips (Fig. 4B,C). Thus, the phosphorylation of Gβ appears to decrease its affinity for the chemotropic complex and destabilize the association of Spa2 with the polarisome. This suggests an explanation for the confined wandering observed in Gβ^{P-} *bud1*Δ cells.

Immediately after exposure to pheromone, the activated receptor and G-protein are distributed almost uniformly on the plasma membrane, as are the first chemotropic and polarisome complexes to be assembled. As the receptor polarizes, however, so do Gα and Gβγ, leading to the eventual concentration of the signaling proteins at the incipient shmoo site. The high density of free Gβγ in this area biases the recruitment of Far1–Cdc24, and thus the localized formation of the chemotropic complex. Moreover, as chemotropic complexes dissociate, they are much more likely to reassemble where free Gβγ is concentrated. The half-life of the chemotropic complex is critical. If it is too short, the cell will not be able to initiate polarized growth. If it is too long, the complex will wander out of the region of high-density receptor and G-protein before the axis of polarity is established. In WT cells, phosphorylation of Gβ decreases the half-life of the complex, thereby limiting the distance it can move before dissociating. This increases the chance that the complex components will reassemble within the active growth area, where receptor and G-protein concentration are highest. In Gβ^{P-} cells, on the other hand, the half-life of the complex is long enough to allow movement across the entire region of high-density receptor and G-protein. Additionally, the zone of Gβ appears to be less well consolidated in Gβ^{P-} cells (Table 2; Fig. 3). A key aspect in this scenario is the recycling of the G-protein – the re-association of the heterotrimer with the receptor. Gβγ cannot report the position of active receptor until it releases from the chemotropic complex and binds inactive Gα. Conversely, the chemotropic complexes can move away from the growth site, blind to local Gβγ density, as long as they remain intact. Interestingly, mutations that disrupt the interaction of Gβ with the N-terminal interface of Gα, or prevent inactivation of Gα, also implicate G-protein cycling in chemotropic shmooing (Strickfaden and Pryciak, 2008). We infer that by increasing the rate at which the position of the activated receptor is reported, the Gα-GDP/GTP and the Gβ-phosphorylation/dephosphorylation cycles strengthen the indirect link between the receptor and the chemotropic complex, and consequently influence the position of the polarity proteins. Posttranslational modification of Gβ may therefore extend the well-established paradigm that cycling is central to the function of G-proteins.

Polarization of Gβ

Our results suggest that Gβ phosphorylation is critical for pheromone-induced Gβ polarization (Fig. 3; Table 2). Although the GFP–Gβ^{P-} polarization defect could result simply from the drifting axis of polarity, a number of observations raise a more interesting possibility: Gβ phosphorylation could play a key role in the genesis of pheromone-induced intracellular signaling gradients. Given that full pheromone-induced phosphorylation of Gβ depends on Fus3 and on Gα–Fus3 interaction (Metodiev et al., 2002), and that gradients of active Fus3 emanate from the tips of shmooing cells (Maeder et al., 2007), we propose that Gα recruits Fus3 to phosphorylate Gβ at the incipient shmoo site. As it is also known that pheromone-induced polarization of Gα and Gβ requires their co-internalization with the receptor (Suchkov

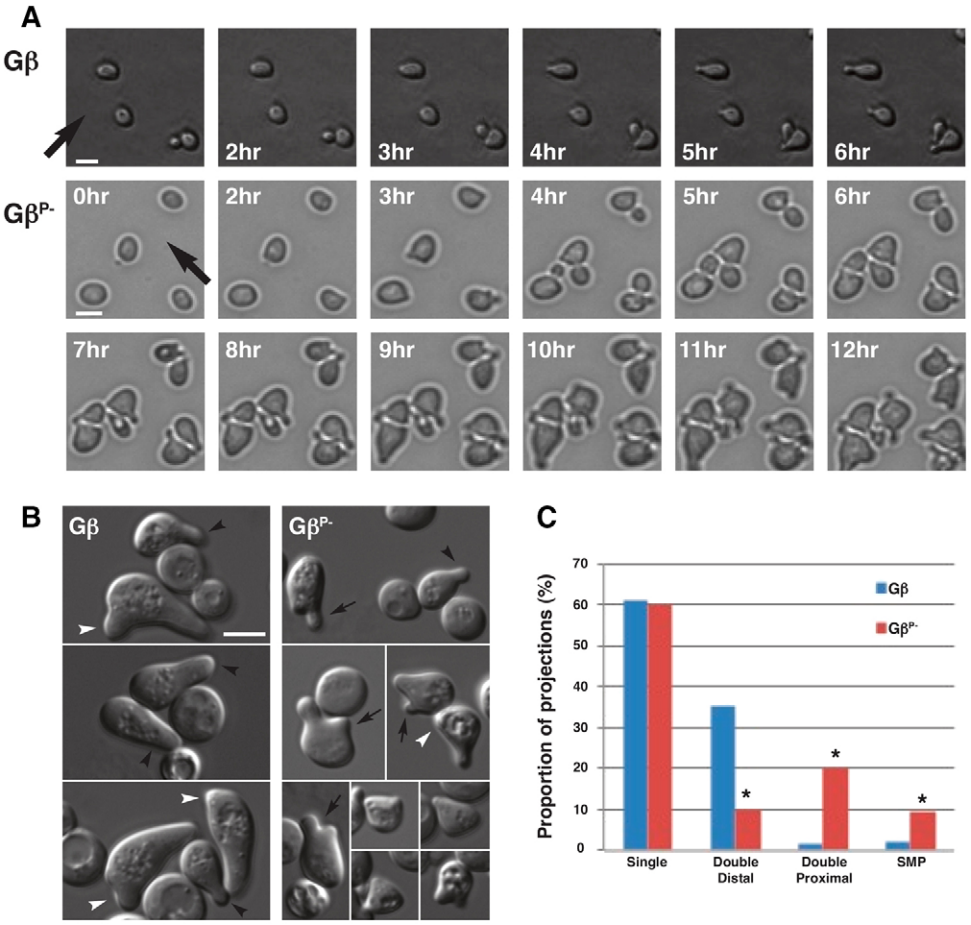

Fig. 6. Gβ^{P-} confers chemotropic growth defects in both artificial and natural pheromone gradients. (**A**) Gβ^{P-} *BUD1* cells cannot properly orient and stabilize polarized growth in an artificial pheromone gradient. Representative time-lapse images of gradient-stimulated WT and Gβ^{P-} cells in a microfluidic device are shown. Black arrows indicate the direction of the gradient. The mean±s.e.m.of the orientation angle for the first protrusions formed by Gβ^{P-} cells was 89.9±4.2°(n=314), as compared to 56.9±4.6°(n=83) for WT shmoos (Brett et al., 2012), where 90° indicates random orientation. (**B**) Gβ^{P-} *BUD1* cells in mating mixtures exhibit shmoo defects similar to Gβ^{P-} *bud1*Δ cells exposed to isotropic pheromone. Representative images of cells from bilateral Gβ *BUD1* and Gβ^{P-} *BUD1* mating mixtures after 5 hours. Black arrowheads indicate cells scored as single shmoos; white arrowheads indicate distal double projections; and black arrows indicate proximal double projections. Small squares show examples of SMP cells. (**C**) Quantification of the shmoo types found in the WT and Gβ^{P-} bilateral mating mixtures. The percentages of shmooed cells in each class are shown in the bar graph. *P<0.0001 for the comparison Gβ versus Gβ^{P-} in each class; n=300 for both strains. Similar results were obtained in each of three trials. Scale bars: 5 μm.

et al., 2010), it will be interesting to determine whether unphosphorylated Gβ is preferentially internalized along with Gα and the receptor while phosphorylated Gβ is left on the membrane. A synergistic combination of these two mechanisms – localized Gβ phosphorylation at the shmoo site and preferential internalization of unphosphorylated Gβ at the back of the cell – would be expected to rapidly generate a steep gradient of phosphorylated Gβ via what is essentially a LEGI-type mechanism. An intracellular gradient of phosphorylated Gβ underlying yeast chemotropism would provide an interesting analogy to the intracellular gradient of the phosphorylated lipid, PIP_3, found in numerous chemotactic systems (Jin et al., 2000; Servant et al., 2000; Comer and Parent, 2002).

Role of Gβ phosphorylation in chemotropism

To determine whether Gβ phosphorylation contributes to directional sensing in addition to its role in mating projection formation, we examined how Gβ^{P-} affects chemotropism in both natural and artificial pheromone gradients. These experiments were performed with *BUD1* strains, as we wished to determine how well the chemotropic shmoo pathway would override the default shmoo pathway to orient and sustain growth up a gradient. In mating mixtures, Gβ^{P-} conferred defects in initial orientation (Fig. 5A) and polarized growth (Fig. 6B). Similar but more pronounced defects were observed in artificial pheromone gradients (Fig. 6A). Remarkably, the polarized growth defects were gradient-specific. Gβ^{P-} cells formed mating projections when treated with isotropic pheromone, but could not maintain polarized growth –even at the default site – in either artificial or natural gradients. It is noteworthy that the types and proportions of aberrant shmoos formed by Gβ^{P-} *BUD1* cells in mating mixtures were very similar to those formed by Gβ^{P-} *bud1*Δ cells in isotropic pheromone (compare Fig. 6B,C and Fig. 1B,C). In both cases, the cells were forced to use the chemotropic pathway without being able to phosphorylate Gβ. The resulting defects reveal that the cells attempt to shmoo chemotropically, but cannot maintain a stable axis of polarity. These data strongly suggest that Gβ phosphorylation is critical for the initial positioning and maintenance of the chemotropic growth site.

In addition to mechanisms that establish and stabilize directional growth, chemotroping cells must have a means to alter their direction and track dynamic gradients in mating mixtures. To successfully fuse with the shmoo tip of a partner, a yeast cell must not only determine the direction of the strongest source of pheromone and orient its growth accordingly, it must continually reassess the position of the target cell while ignoring weaker signals. The shape of the gradient and concentration of pheromone most likely change as the two cells grow towards each other, and as zygotes form in the mating mixture. Although the mechanisms underlying reorientation are unknown, it is easy to appreciate that the establishment of a chemotropic growth site and ongoing adjustments to its position pose distinct challenges. To date, only one mutation that specifically affects reorientation has been reported: *ste2*^{T236} (Vallier et al., 2002). It is therefore of

Journal of Cell Science

Journal of Cell Science

considerable interest that $G\beta^{P-}$ confers a dramatic defect in reorientation. This suggests that Gβ phosphorylation plays a critical role in gradient tracking.

In summary, we propose that the phosphorylation of Gβ contributes to chemotropism in two ways: (1) Gβ modification is used to rapidly generate a signaling gradient in which phosphorylated Gβ is concentrated at the incipient shmoo site. This may facilitate the amplification of other intracellular signaling gradients; (2) Phosphorylation of Gβ decreases its affinity for Far1 and perhaps other chemotropic components, thereby shortening the cycle time between the receptor and polarisome. More frequent updating of receptor status increases sensitivity to changes in the pheromone gradient.

Materials and Methods

Molecular and microbiological techniques

Standard methods were used for microbial and molecular manipulation (Sherman et al., 1986; Ausubel et al., 1994; Guthrie and Fink, 2002). Strains and plasmids used are listed in supplementary material Tables S1 and S2, respectively. Yeast cells were cultured in rich medium (YEPD) at 30℃ unless noted otherwise.

Spa2–GFP localization in isotropic pheromone

*MAT***a** *bud1*Δ Gβ or $G\beta^{P-}$ cells expressing *SPA2-GFP* were incubated together on s.d. complete agar pads containing 150 nM α-factor; one strain was labeled with ConA-Alexa Fluor 594 (Molecular Probes). Six fields were imaged at 15-minute intervals with 0.5 μm *z*-sections acquired using a DeltaVision deconvolution system (Applied Precision) on an Olympus IX-70 microscope with an NA 1.4×60 objective. The images were deconvolved using Huygens Deconvolution Software V. 3.7 (Scientific Volume Imaging), sum projected (GFP), or average projected (DIC), and converted into 8-bit TIF files using ImageJ. The scale bar equals 5 μm in all images.

Spa2–GFP time-lapse microscopy in mating mixtures

WT *MAT*α cells were labeled with ConA-Alexa Fluor 594 prior to mixing with *MAT***a** *bud1*Δ Gβ or $G\beta^{P-}$ cells expressing *SPA2-GFP*. Mating mixtures were incubated on s.d. complete agar pads. Images were acquired 25 minutes after mixing and at 15-minute intervals thereafter. Image acquisition and analysis was as described above. Tracking analysis was performed using the ImageJ Manual Tracking plugin.

GFP–Gβ time-lapse microscopy in isotropic pheromone conditions

*MAT***a** *bud1*Δ GFP–Gβ and *MAT***a** *bud1*Δ GFP–$G\beta^{P-}$ cells were incubated together on s.d. complete agar pads containing 150 nM α-factor. The strains were distinguished by labeling one or the other with ConA-Alexa Fluor 594. Cells were first imaged 15 minutes after exposure to pheromone and at 10-minute intervals thereafter. Six fields were imaged at each time point with 15 0.3 μm z-section acquired using an ANDOR Revolution XD spinning disk laser confocal system with a motorized Olympus IX-81 microscope, a Yokogawa CSU-X1 spinning disk unit, motorized XYZ control (piezo) and an iXon897 EMCCD camera, all controlled by Andor iQ2 software. A UplanSApo NA 1.4×100 objective was used with 488-nm laser excitation. Voxel size was 133×133×280 nm. An Okolab chamber was used to maintain cells at 30℃. The images were then sum projected and converted into 8-bit TIF files using ImageJ and false colored. The intensity profile along the major axis of the cells was quantified using BudPolarity (Vernay et al., 2012). The line graphs in Fig. 3 represent the output from this analysis. In Table 2, cells were scored as exhibiting polarized Gβ if they met all of the following criteria: peak signal intensity ≥2× the baseline value over less than one half the cell surface for at least three consecutive time points. Cells were scored as exhibiting polarized growth when they were judged to be elongating predominantly along one axis at the center of the DIC z-stack. The ImageJ ellipse tool was used for this determination.

GFP–Gβ time-lapse microscopy in mating mixtures

WT *MAT*α cells were mixed 1:1 with *MAT***a** *bud1*Δ GFP–Gβ or *MAT***a** *bud1*Δ GFP–$G\beta^{P-}$ cells. Mating mixtures were incubated on s.d. complete agar pads and images were acquired every 15 minutes. Image acquisition and analysis were identical to that described for isotropic pheromone conditions. In Table 2, cells were scored as exhibiting polarized Gβ if they met all of the following criteria: peak signal intensity ≥1.5× the baseline value over less than one half the cell surface for at least three consecutive time points. Cells were scored as exhibiting polarized growth as described above.

FRAP analysis of Spa2–GFP

*MAT***a** *bud1*Δ Gβ or $G\beta^{P-}$ cells expressing *SPA2-GFP* were grown to mid-log phase and then exposed to 30 nM α-factor at 30℃ for 1 hour. FRAP analysis was carried out on a Zeiss LSM 510 META confocal Axiovert 200M microscope (Carl Zeiss) using an NA 1.4×63 Plan-Apo objective and 488-nm LASER excitation. Images were captured every 1 second at 2–5% maximum laser intensity and 10×0.5 milliseconds photobleaching scans at 100% laser intensity were performed on a circular area of 1 μm^2 at the shmoo tip. Data analysis was carried out as described (Bassilana and Arkowitz, 2006).

iFRAP analysis of GFP–Cdc42

*MAT***a** *bud1*Δ Gβ or $G\beta^{P-}$ cells expressing *GFP-CDC42* were grown to mid-log phase and exposed to 30 nM α-factor at 30℃ for 1 hour. iFRAP was carried out as described for FRAP analyses except that the cell body was photobleached rather than the shmoo tip. The average intensity of the bleached or unbleached area was normalized for photobleaching during image acquisition, using the average intensity of the cell with MatLab. Loss of fluorescence intensity was then fitted to an exponential curve.

Mating projection assays

To study mating projection formation and maintenance under isotropic pheromone conditions, mid-log phase cells were exposed to α-factor at the concentrations and times indicated. DIC images for experiments carried out in liquid cultures were acquired using a Zeiss Axioskop 2 microscope fitted with an NA 1.4×63 Plan-Apo oil immersion objective and a Zeiss AxioCam digital camera, and processed with Zeiss AxioVision software. To study mating projection formation and maintenance in physiological pheromone gradients, cultures were grown to mid-log phase at 30℃ in YEPD. Dilute bilateral Gβ and $G\beta^{P-}$ mating mixtures containing ~1×10^7 *MAT*α cells and ~1×10^7 *MAT***a** cells were then spread on YEPD agar. Time points were taken at 1 hour intervals for 5 hours, fixed with 3.7% formaldehyde, and 630×DIC images of shmoos were acquired using the Zeiss equipment described above. Mating projection lengths were measured using ImageJ. Percentages in each shmoo class were scored on a hemocytometer using a Leitz Laborlutz S phase-contrast microscope fitted with an NA 0.65×40 Plan objective.

Orientation assays

To measure the ability of cells to orient their growth in physiological pheromone gradients, cultures were grown to mid-log phase. Dilute bilateral Gβ and $G\beta^{P-}$ mating mixtures containing ~5×10^6 *MAT*α cells and ~5×10^6 *MAT***a** cells were then incubated for 3 hours on filters (0.45 μm Millipore) placed on YEPD agar. Filters were washed in 1 ml sterile H_2O to harvest cells. 630×DIC images of zygotes were acquired using the Zeiss Axioskop 2 microscope and camera described above. Zygote angles were measured using ImageJ. The response of cells to artificial pheromone gradients was assayed using a microfluidic device, as described (Brett et al., 2012).

Reorientation assay

Mid-log phase liquid cultures containing ~10^7 *MAT*α cells and ~10^7 *MAT***a** cells were shaken at 250 r.p.m. at 30℃ for 3 hours to induce shmooing prior to mating. Cultures of either WT *MAT*α and *MAT***a** cells or $G\beta^{P-}$ *MAT*α and *MAT***a** cells were then spread onto YEPD agar and incubated for 3 hours. Images of zygotes were collected using an Olympus BH-2 inverted microscope fitted with a CDPlan 40 objective and an Olympus digital camera (magnification 400×). Zygote angles were measured using ImageJ.

Statistics

The *P*-values for the comparisons of length, angle and time measurements were determined using unpaired, two-tailed *t*-tests (Graphpad). The *P*-values for the comparisons of percentages were determined using the chi-square test (Graphpad).

Acknowledgements

The authors would like to thank Jayme Dyer and Daniel Lew for yeast strains and plasmids, for helpful discussions and for communicating results prior to publication.

Author contributions

R.D.F. participated in the experimental design, and performed experiments and data analysis, as well as constructing all of the figures; M.-E.B. performed the experiment shown in Fig. 6A along with D.E.; N.W. did the pull-down/mass spectrometry sample preparation for the experiments represented in supplementary material Fig. S2; M.V.M. ran and analyzed the mass spectrometry data and also first made the observation depicted in Fig. 1A; E.A. performed experiments and quantified the data; O.D. designed and performed the experiment shown in supplementary material Fig. S1; R.A. helped design and perform the experiments, as well

contributing to the formulation and editing of the manuscript; and D.S. directed the project and wrote the manuscript.

Funding

This work was supported by the National Science Foundation (NSF) [grant numbers MCB-0453964 and MCB1024718 to D.E.S.]. R.D. was supported by European Molecular Biology Organization (EMBO) [grant number ASTF 196.00-2009] and Eiffel [grant number 690570F] fellowships. Work in R.A.'s laboratory was supported by the Centre national de la recherche scientifique (CNRS), Fondation pour la Recherche Medicale (FRM)-BNP-Paribas, the French National Research Agency [grant number ANR-09-BLAN-0299-01] and the French Cancer Research Association (ARC) [grant number SFI20121205755].

Supplementary material available online at
http://jcs.biologists.org/lookup/suppl/doi:10.1242/jcs.112797/-/DC1

References

Alldridge, L., Metodieva, G., Greenwood, C., Al-Janabi, K., Thwaites, L., Sauven, P. and Metodiev, M. (2008). Proteome profiling of breast tumors by gel electrophoresis and nanoscale electrospray ionization mass spectrometry. *J. Proteome Res.* **7**, 1458-1469.

Arkowitz, R. A. (2009). Chemical gradients and chemotropism in yeast. *Cold Spring Harb. Perspect. Biol.* **1**, a001958.

Arkowitz, R. A. and Lowe, N. (1997). A small conserved domain in the yeast Spa2p is necessary and sufficient for its polarized localization. *J. Cell Biol.* **138**, 17-36.

Ausubel, F. M., Brent, R., Kingston, R. E., Moore, D. D., Seidman, J. G., Smith, J. A. and Struhl, K. (1994). *Current Protocols in Molecular Biology*. John Wiley and Sons, Inc.

Ballon, D. R., Flanary, P. L., Gladue, D. P., Konopka, J. B., Dohlman, H. G. and Thorner, J. (2006). DEP-domain-mediated regulation of GPCR signaling responses. *Cell* **126**, 1079-1093.

Bar, E. E., Ellicott, A. T. and Stone, D. E. (2003). Gbetagamma recruits Rho1 to the site of polarized growth during mating in budding yeast. *J. Biol. Chem.* **278**, 21798-21804.

Barale, S., McCusker, D. and Arkowitz, R. A. (2006). Cdc42p GDP/GTP cycling is necessary for efficient cell fusion during yeast mating. *Mol. Biol. Cell* **17**, 2824-2838.

Bardwell, L. (2005). A walk-through of the yeast mating pheromone response pathway. *Peptides* **26**, 339-350.

Basile, J. R., Barac, A., Zhu, T., Guan, K. L. and Gutkind, J. S. (2004). Class IV semaphorins promote angiogenesis by stimulating Rho-initiated pathways through plexin-B. *Cancer Res.* **64**, 5212-5224.

Bassilana, M. and Arkowitz, R. A. (2006). Rac1 and Cdc42 have different roles in Candida albicans development. *Eukaryot. Cell* **5**, 321-329.

Bidlingmaier, S. and Snyder, M. (2004). Regulation of polarized growth initiation and termination cycles by the polarisome and Cdc42 regulators. *J. Cell Biol.* **164**, 207-218.

Brett, M.-E., DeFlorio, R., Stone, D. E. and Eddington, D. T. (2012). A microfluidic device that forms and redirects pheromone gradients to study chemotropism in yeast. *Lab Chip* **12**, 3127-3134.

Butty, A. C., Pryciak, P. M., Huang, L. S., Herskowitz, I. and Peter, M. (1998). The role of Far1p in linking the heterotrimeric G protein to polarity establishment proteins during yeast mating. *Science* **282**, 1511-1516.

Chakrabarti, S. and Gintzler, A. R. (2003). Phosphorylation of Gbeta is augmented by chronic morphine and enhances Gbetagamma stimulation of adenylyl cyclase activity. *Brain Res. Mol. Brain Res.* **119**, 144-151.

Cismowski, M. J., Metodiev, M. V., Draper, E. M. and Stone, D. E. (2001). Biochemical analysis of yeast G(α) mutants that enhance adaptation to pheromone. *Biochem. Biophys. Res. Commun.* **284**, 247-254.

Cole, G. M. and Reed, S. I. (1991). Pheromone-induced phosphorylation of a G protein β subunit in S. cerevisiae is associated with an adaptive response to mating pheromone. *Cell* **64**, 703-716.

Cole, G. M., Stone, D. E. and Reed, S. I. (1990). Stoichiometry of G protein subunits affects the Saccharomyces cerevisiae mating pheromone signal transduction pathway. *Mol. Cell. Biol.* **10**, 510-517.

Comer, F. I. and Parent, C. A. (2002). PI 3-kinases and PTEN: how opposites chemoattract. *Cell* **109**, 541-544.

Cox, J. and Mann, M. (2008). MaxQuant enables high peptide identification rates, individualized p.p.b.-range mass accuracies and proteome-wide protein quantification. *Nat. Biotechnol.* **26**, 1367-1372.

Cox, J., Neuhauser, N., Michalski, A., Scheltema, R. A., Olsen, J. V. and Mann, M. (2011). Andromeda: a peptide search engine integrated into the MaxQuant environment. *J. Proteome Res.* **10**, 1794-1805.

Daniels, K. J., Srikantha, T., Lockhart, S. R., Pujol, C. and Soll, D. R. (2006). Opaque cells signal white cells to form biofilms in Candida albicans. *EMBO J.* **25**, 2240-2252.

Devreotes, P. and Janetopoulos, C. (2003). Eukaryotic chemotaxis: distinctions between directional sensing and polarization. *J. Biol. Chem.* **278**, 20445-20448.

Dohlman, H. G. and Thorner, J. W. (2001). Regulation of G protein-initiated signal transduction in yeast: paradigms and principles. *Annu. Rev. Biochem.* **70**, 703-754.

Dorer, R., Pryciak, P. M. and Hartwell, L. H. (1995). Saccharomyces cerevisiae cells execute a default pathway to select a mate in the absence of pheromone gradients. *J. Cell Biol.* **131**, 845-861.

Draper, E., Dubrovskyi, O., Bar, E. E. and Stone, D. E. (2009). Dse1 may control cross talk between the pheromone and filamentation pathways in yeast. *Curr. Genet.* **55**, 611-621.

Dyer, J. M., Savage, N. S., Jin, M., Zyla, T. R., Elston, T. C. and Lew, D. J. (2013). Tracking shallow chemical gradients by actin-driven wandering of the polarization site. *Curr. Biol.* **23**, 32-41.

English, D., Garcia, J. G. and Brindley, D. N. (2001). Platelet-released phospholipids link haemostasis and angiogenesis. *Cardiovasc. Res.* **49**, 588-599.

Evangelista, M., Pruyne, D., Amberg, D. C., Boone, C. and Bretscher, A. (2002). Formins direct Arp2/3-independent actin filament assembly to polarize cell growth in yeast. *Nat. Cell Biol.* **4**, 260-269.

Feng, Y., Song, L. Y., Kincaid, E., Mahanty, S. K. and Elion, E. A. (1998). Functional binding between Gbeta and the LIM domain of Ste5 is required to activate the MEKK Ste11. *Curr. Biol.* **8**, 267-282.

Ghaemmaghami, S., Huh, W.-K., Bower, K., Howson, R. W., Belle, A., Dephoure, N., O'Shea, E. K. and Weissman, J. S. (2003). Global analysis of protein expression in yeast. *Nature* **425**, 737-741.

Greenwood, C., Metodieva, G., Al-Janabi, K., Lausen, B., Alldridge, L., Leng, L., Bucala, R., Fernandez, N. and Metodiev, M. V. (2012). Stat1 and CD74 overexpression is co-dependent and linked to increased invasion and lymph node metastasis in triple-negative breast cancer. *J. Proteomics* **75**, 3031-3040.

Guthrie, C. and Fink, G. R. (2002). *Guide to Yeast Genetics and Molecular Biology*. San Diego, CA: Academic Press.

Heinecke, N. L., Pratt, B. S., Vaisar, T. and Becker, L. (2010). PepC: proteomics software for identifying differentially expressed proteins based on spectral counting. *Bioinformatics* **26**, 1574-1575.

Hong, K. and Nishiyama, M. (2010). From guidance signals to movement: signaling molecules governing growth cone turning. *Neuroscientist* **16**, 65-78.

Howell, A. S., Savage, N. S., Johnson, S. A., Bose, I., Wagner, A. W., Zyla, T. R., Nijhout, H. F., Reed, M. C., Goryachev, A. B. and Lew, D. J. (2009). Singularity in polarization: rewiring yeast cells to make two buds. *Cell* **139**, 731-743.

Iijima, M., Huang, Y. E. and Devreotes, P. (2002). Temporal and spatial regulation of chemotaxis. *Dev. Cell* **3**, 469-478.

Jackson, C. L. and Hartwell, L. H. (1990). Courtship in S. cerevisiae: both cell types choose mating partners by responding to the strongest pheromone signal. *Cell* **63**, 1039-1051.

Jin, T., Zhang, N., Long, Y., Parent, C. A. and Devreotes, P. N. (2000). Localization of the G protein betagamma complex in living cells during chemotaxis. *Science* **287**, 1034-1036.

Kang, P. J., Béven, L., Hariharan, S. and Park, H. O. (2010). The Rsr1/Bud1 GTPase interacts with itself and the Cdc42 GTPase during bud-site selection and polarity establishment in budding yeast. *Mol. Biol. Cell* **21**, 3007-3016.

Kim, J., Bortz, E., Zhong, H., Leeuw, T., Leberer, E., Vershon, A. K. and Hirsch, J. P. (2000). Localization and signaling of G(β) subunit Ste4p are controlled by a-factor receptor and the a-specific protein Asg7p. *Mol. Cell. Biol.* **20**, 8826-8835.

Kim, S., Dong, J. and Lord, E. M. (2004). Pollen tube guidance: the role of adhesion and chemotropic molecules. *Curr. Top. Dev. Biol.* **61**, 61-79.

Li, E., Cismowski, M. J. and Stone, D. E. (1998a). Phosphorylation of the pheromone-responsive Gbeta protein of Saccharomyces cerevisiae does not affect its mating-specific signaling function. *Mol. Gen. Genet.* **258**, 608-618.

Li, E., Meldrum, E., Stratton, H. F. and Stone, D. E. (1998b). Substitutions in the pheromone-responsive Gbeta protein of Saccharomyces cerevisiae confer a defect in recovery from pheromone treatment. *Genetics* **148**, 947-961.

Maeder, C. I., Hink, M. A., Kinkhabwala, A., Mayr, R., Bastiaens, P. I. and Knop, M. (2007). Spatial regulation of Fus3 MAP kinase activity through a reaction-diffusion mechanism in yeast pheromone signalling. *Nat. Cell Biol.* **9**, 1319-1326.

Matheos, D., Metodiev, M., Muller, E., Stone, D. and Rose, M. D. (2004). Pheromone-induced polarization is dependent on the Fus3p MAPK acting through the formin Bni1p. *J. Cell Biol.* **165**, 99-109.

Mato, J. M., Losada, A., Nanjundiah, V. and Konijn, T. M. (1975). Signal input for a chemotactic response in the cellular slime mold Dictyostelium discoideum. *Proc. Natl. Acad. Sci. USA* **72**, 4991-4993.

Metodiev, M. V. (2011). Applications of nanoscale liquid chromatography coupled to Tandem mass spectrometry in quantitative studies of protein expression, protein-protein interaction, and protein phosphorylation. *Methods Mol. Biol.* **790**, 99-113.

Metodiev, M. V., Matheos, D., Rose, M. D. and Stone, D. E. (2002). Regulation of MAPK function by direct interaction with the mating-specific Galpha in yeast. *Science* **296**, 1483-1486.

Moore, T. I., Chou, C. S., Nie, Q., Jeon, N. L. and Yi, T. M. (2008). Robust spatial sensing of mating pheromone gradients by yeast cells. *PLoS ONE* **3**, e3865.

Nern, A. and Arkowitz, R. A. (1998). A GTP-exchange factor required for cell orientation. *Nature* **391**, 195-198.

Nern, A. and Arkowitz, R. A. (1999). A Cdc24p-Far1p-Gbetagamma protein complex required for yeast orientation during mating. *J. Cell Biol.* **144**, 1187-1202.

Nern, A. and Arkowitz, R. A. (2000). G proteins mediate changes in cell shape by stabilizing the axis of polarity. *Mol. Cell* **5**, 853-864.

Palanivelu, R. and Preuss, D. (2000). Pollen tube targeting and axon guidance: parallels in tip growth mechanisms. *Trends Cell Biol.* **10**, 517-524.

Park, H. O., Bi, E., Pringle, J. R. and Herskowitz, I. (1997). Two active states of the Ras-related Bud1/Rsr1 protein bind to different effectors to determine yeast cell polarity. *Proc. Natl. Acad. Sci. USA* **94**, 4463-4468.

Pruyne, D. and Bretscher, A. (2000a). Polarization of cell growth in yeast. *J. Cell Sci.* **113**, 571-585.

Pruyne, D. and Bretscher, A. (2000b). Polarization of cell growth in yeast. I. Establishment and maintenance of polarity states. *J. Cell Sci.* **113**, 365-375.

Reed, S. I., Hadwiger, J. A. and Lörincz, A. T. (1985). Protein kinase activity associated with the product of the yeast cell division cycle gene CDC28. *Proc. Natl. Acad. Sci. USA* **82**, 4055-4059.

Sagot, I., Klee, S. K. and Pellman, D. (2002). Yeast formins regulate cell polarity by controlling the assembly of actin cables. *Nat. Cell Biol.* **4**, 42-50.

Segall, J. E. (1993). Polarization of yeast cells in spatial gradients of alpha mating factor. *Proc. Natl. Acad. Sci. USA* **90**, 8332-8336.

Servant, G., Weiner, O. D., Herzmark, P., Balla, T., Sedat, J. W. and Bourne, H. R. (2000). Polarization of chemoattractant receptor signaling during neutrophil chemotaxis. *Science* **287**, 1037-1040.

Sherman, F., Fink, G. R. and Hicks, J. B. (ed.) (1986). *Laboratory Course Manual For Methods in Yeast Genetics*. Cold Spring Harbor, NY: Cold Spring Harbor Laboratory Press.

Snetselaar, K. M., Bolker, M. and Kahmann, R. (1996). Ustilago maydis Mating Hyphae Orient Their Growth toward Pheromone Sources. *Fungal Genet. Biol.* **20**, 299-312.

Stratton, H. F., Zhou, J., Reed, S. I. and Stone, D. E. (1996). The mating-specific G(α) protein of Saccharomyces cerevisiae downregulates the mating signal by a mechanism that is dependent on pheromone and independent of G(β)(γ) sequestration. *Mol. Cell. Biol.* **16**, 6325-6337.

Strickfaden, S. C. and Pryciak, P. M. (2008). Distinct roles for two Galpha-Gbeta interfaces in cell polarity control by a yeast heterotrimeric G protein. *Mol. Biol. Cell* **19**, 181-197.

Suchkov, D. V., DeFlorio, R., Draper, E., Ismael, A., Sukumar, M., Arkowitz, R. and Stone, D. E. (2010). Polarization of the yeast pheromone receptor requires its internalization but not actin-dependent secretion. *Mol. Biol. Cell* **21**, 1737-1752.

Tojima, T., Hines, J. H., Henley, J. R. and Kamiguchi, H. (2011). Second messengers and membrane trafficking direct and organize growth cone steering. *Nat. Rev. Neurosci.* **12**, 191-203.

Tranquillo, R. T., Lauffenburger, D. A. and Zigmond, S. H. (1988). A stochastic model for leukocyte random motility and chemotaxis based on receptor binding fluctuations. *J. Cell Biol.* **106**, 303-309.

Vallier, L. G., Segall, J. E. and Snyder, M. (2002). The alpha-factor receptor C-terminus is important for mating projection formation and orientation in Saccharomyces cerevisiae. *Cell Motil. Cytoskeleton* **53**, 251-266.

Valtz, N., Peter, M. and Herskowitz, I. (1995). FAR1 is required for oriented polarization of yeast cells in response to mating pheromones. *J. Cell Biol.* **131**, 863-873.

Vernay, A., Schaub, S., Guillas, I., Bassilana, M. and Arkowitz, R. A. (2012). A steep phosphoinositide bis-phosphate gradient forms during fungal filamentous growth. *J. Cell Biol.* **198**, 711-730.

Wach, A. (1996). PCR-synthesis of marker cassettes with long flanking homology regions for gene disruptions in S. cerevisiae. *Yeast* **12**, 259-265.

Weiner, O. D. (2002). Regulation of cell polarity during eukaryotic chemotaxis: the chemotactic compass. *Curr. Opin. Cell Biol.* **14**, 196-202.

Whiteway, M., Hougan, L. and Thomas, D. Y. (1990). Overexpression of the STE4 gene leads to mating response in haploid Saccharomyces cerevisiae. *Mol. Cell. Biol.* **10**, 217-222.

Wiget, P., Shimada, Y., Butty, A. C., Bi, E. and Peter, M. (2004). Site-specific regulation of the GEF Cdc24p by the scaffold protein Far1p during yeast mating. *EMBO J.* **23**, 1063-1074.

Yu, L., Qi, M., Sheff, M. A. and Elion, E. A. (2008). Counteractive control of polarized morphogenesis during mating by mitogen-activated protein kinase Fus3 and G1 cyclin-dependent kinase. *Mol. Biol. Cell* **19**, 1739-1752.

Journal of Cell Science

Figure S1

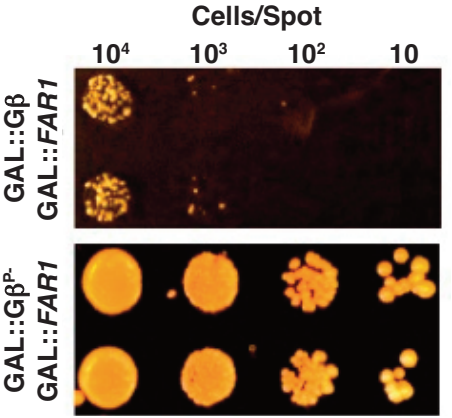

Figure S1. Gβ overexpression genetic assay. 15Dau *bar1*Δ cultures co-transformed with pESC/GAL1-FAR1 and either YCplac111/GAL1-STE4 or YCplac111/GAL1- STE4$^{T320A\ S335A}$ were grown to mid-log phase (~10^7 cells/ml) in selective sucrose medium. 10-fold serial dilutions from 10^5 to 1 were then spotted on selective galactose medium (to induce the overexpression of Far1, and Gβ or Gβ^{P-}) and selective glucose medium (to repress *GAL1*-driven gene expression), and incubated at 30˚C for 48 hr. Ten transformants of each strain were tested. Results for two representative strains of each type are shown. Far1 overexpression rescued overexpression of Gβ^{P-} but not of Gβ. All strains grew similarly on glucose-containing medium.

Figure S2

A

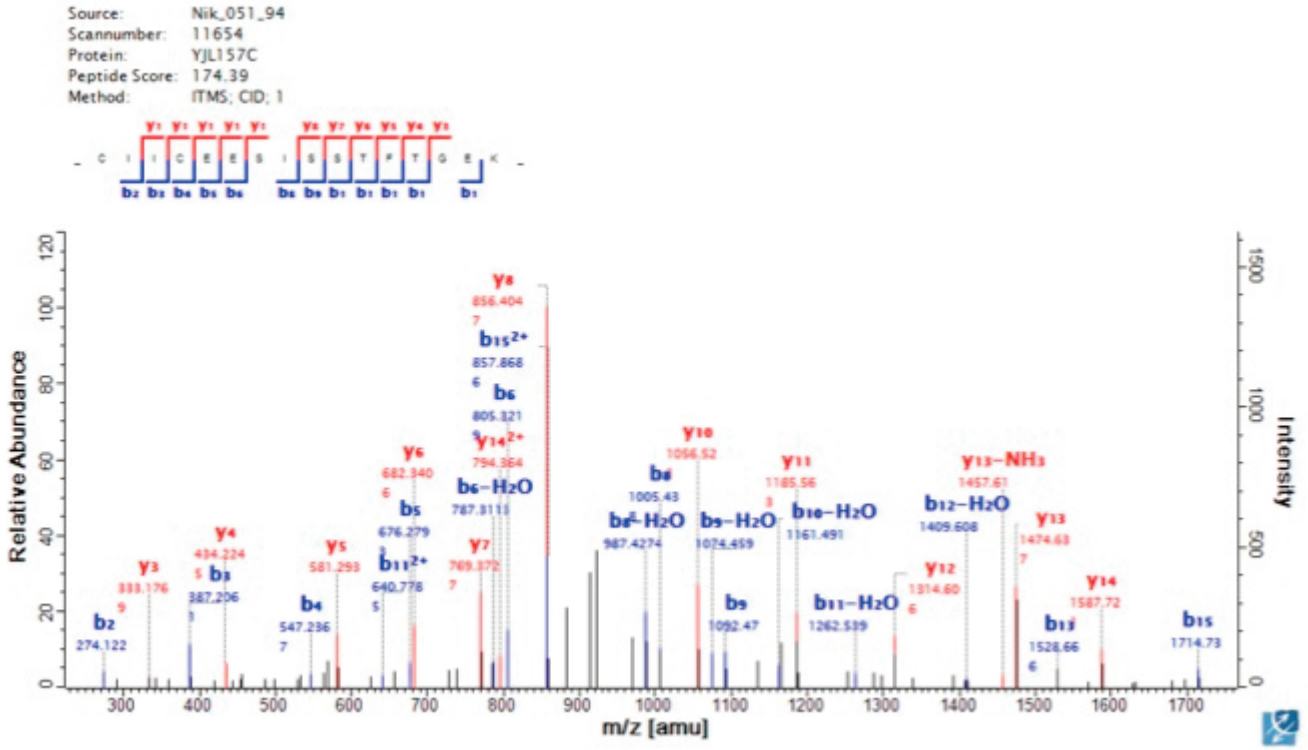
Source: Nik_051_94
Scannumber: 11654
Protein: YJL157C
Peptide Score: 174.39
Method: ITMS; CID; 1
Relative Abundance
Intensity
m/z [amu]

B

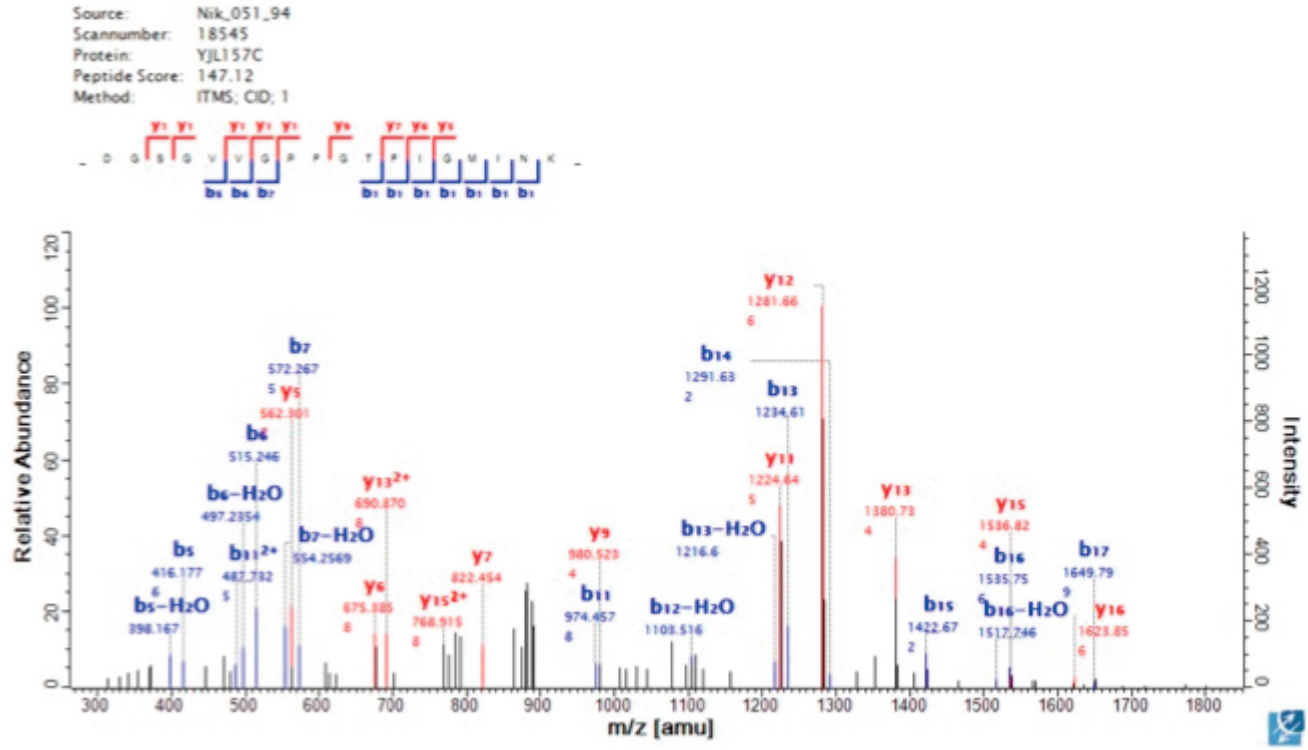
Source: Nik_051_94
Scannumber: 18545
Protein: YJL157C
Peptide Score: 147.12
Method: ITMS; CID; 1
Relative Abundance
Intensity
m/z [amu]

Figure S1. Detection of Far1 in the $G\beta^{P}\gamma$ pull-down. Pull-downs were performed as described in Cismowski et al. (2001). The proteins eluted from the Ni-NTA beads were separated by SDS-PAGE, digested by trypsin, and analyzed by nano-scale LC-MS/MS as previously described (Alldridge et al., 2008; Metodiev, 2011). The LTQ/Orbitrap Velos was operated in data-dependent mode where the high-resolution Orbitrap analyzer first executed two full scans at a resolution of 30,000 (at 400 m/z), followed by 20 MS/MS scans in the LTQ Velos analyzer to isolate and sequence the 20 most abundant peptide ions (Greenwood et al., 2012). Internal mass calibration was maintained using a lock mass ion of 445.12 m/z. Raw MS/MS data were analyzed by MaxQuant and X! Tandem as described previously (Greenwood et al., 2012; Cox and Mann, 2008; Cox et al., 2011). Each sample was analysed in triplicate by LC-MS/MS. Two high-scoring MS/MS spectra from LC-MS/MS runs analyzing the 94kDa fraction of the $G\beta^{P}\gamma$ pull-down sample are shown. (A) An MS/MS spectrum matching a peptide with sequence **CIICEESISSTFTGEK** from Far1. Andromeda, the search engine of MaxQuant, matched the spectrum to the peptide with a score of 174 and peptide expectation value (PEP) of 1.54E-06. (B) An MS/MS spectrum matching a peptide with sequence **DGSGVVGPFGTFIGMINK** from Far1. Andromeda matched the spectrum to the peptide with a score of 147 and PEP of 3.32E-08. The sequence-specific y and b fragment ion series are shown in red and blue as assigned by MaxQuant. For statistical analysis of spectral count data, the MS/MS data were filtered at 1% FDR at both the peptide and protein levels, and the filtered data was used to quantify the proteins using the spectral counting approach. The significance of the obtained differences in spectral counts reported by MaxQuant or X!Tandem were analyzed by the G-test (Greenwood et al. 2012), which does not require the data to be distributed normally (Heinecke, et al., 2010). Far1 was detected with a total of 19 spectral counts (7, 6, and 6 in the three separate replicates) and with 0 counts in the $G\beta^{P}\gamma$ and WT pull-downs, respectively. If the affinities of $G\beta^{P}\gamma$ and $G\beta\gamma$ for Far1 were similar, the total counts expected for Far1 in the WT pull-down would be 14 rather than 0 after normalizing for the amount of $G\beta\gamma$ on the beads ($p = 0.00013$).

REFERENCES

Alldridge, L., Metodieva, G., Greenwood, C., Al-Janabi, K., Thwaites, L., Sauven, P., and Metodiev, M. (2008). Proteome profiling of breast tumors by gel electrophoresis and nanoscale electrospray ionization mass spectrometry. *J Proteome Res* **7**:1458-69.

Cismowski, M. J., Metodiev, M. V., Draper, E. M. and Stone, D. E. (2001). Biochemical analysis of yeast Gα mutants that enhance adaptation to pheromone. *Biochem. Biophys. Res. Comm.* **284**, 247-254.

Cox, J. and Mann, M. (2008). MaxQuant enables high peptide identification rates, individualized p.p.b.-range mass accuracies and proteome-wide protein quantification. *Nat Biotechnol* **26**, 1367-72.

Cox, J., Neuhauser, N., Michalski, A., Scheltema, R. A., Olsen, J. V., and Mann, M. (2011). Andromeda: a peptide search engine integrated into the MaxQuant environment. *J Proteome Res* **10**, 1794-805.

Greenwood, C., Metodieva, G., Al-Janabi, K., Lausen, B., Alldridge, L., Leng, L., Bucala, R., Fernandez, M., and Metodiev, M. V. (2012). Stat1 and CD74 overexpression is co-dependent and linked to increased invasion and lymph node metastasis in triple-negative breast cancer. *J. Proteomics* **75**, 3031-40.

Heinecke, N. L., Pratt, B. S., Vaisar, T., and Becker, L. (2010). PepC: proteomics software for identifying differentially expressed proteins based on spectral counting. *Bioinformatics* **26**, 1574-5.

Metodiev, M. V. (2011). Applications of nanoscale liquid chromatography coupled to Tandem mass spectrometry in quantitative studies of protein expression, protein-protein interaction, and protein phosphorylation. *Methods Mol Biol* **790**, 99-113.

Supplementary Table 1. Yeast strains used in this study

Strain	Genotype	Source
DSY257	*MAT***a** *bar1Δ ade1 his2 leu2-3, 112 trp1-1a ura3Δ*	Stone lab
ELY104	*MAT***a** *bar1Δ ade1 his2 leu2-3, 112 trp1-1a ura3Δ ste4::URA3*	Stone lab
RDY114	*MAT***a** *ste4$^{T320A\ S335A}$ bar1Δ ade1 his2 leu2-3, 112 trp1-1a ura3Δ*	This study
RDY103	*MAT***a** *bud1Δ::KAN bar1Δ ade1 his2 leu2-3, 112 trp1-1a ura3Δ*	This study
RDY120	*MAT***a** *ste4$^{T320A\ S335A}$ bud1Δ::KAN bar1Δ ade1 his2 leu2-3, 112 trp1-1a ura3Δ*	This study
MMY110	*MAT***a** *gpa1Δ::URA3 bud1Δ::KAN bar1Δ ade1 his2 leu2-3, 112 trp1-1a ura3Δ* YCplac22/*gpa1$^{K21E\ R22E}$*	This study
MMY111	*MAT***a** *gpa1Δ::URA3 bud1Δ::KAN bar1Δ ade1 his2 leu2-3, 112 trp1-1a ura3Δ* YCplac22/*GPA1*	This study
	*MAT***a** *gpa1Δ::URA3 bar1Δ ade1 his2 leu2-3, 112 trp1-1a ura3Δ* YCplac22/*gpa1$^{K21E\ R22E}$*	This study
RDY130	*MAT***a** *ste4::URA3 GFP-STE4::ura3 bud1Δ::KAN bar1Δ ade1 his2 leu2-3, 112 trp1 ura3*	This study
RDY132	*MAT***a** *ste4::URA3 GFP- ste4$^{T320A\ S335A}$::ura3 bud1Δ::KAN bar1Δ ade1 his2 leu2-3, 112 trp1 ura3Δ*	This study
RDY126	*MAT***a** *ste4::URA3 GFP-STE4::ura3 bar1Δ ade1 his2 leu2-3, 112 trp1 ura3*	This study
RDY139	*MAT***a** *ste4::URA3 GFP- ste4$^{T320A\ S335A}$::ura3 bar1Δ ade1 his2 leu2-3, 112 trp1 ura3Δ*	This study
DSY246	*MATα bar1Δ ade1 his2 leu2-3, 112 trp1-1a ura3Δ*	Stone lab

RDY217	*MAT*α *ste4*$^{T320A\ S335A}$ *bar1*Δ *ade1 his2 leu2-3, 112 trp1-1a ura3*Δ	This study
RDY246	*MAT***a** *bud1*Δ::*KAN bar1*Δ *ade1 his2 leu2-3, 112 trp1-1a ura3*Δ pRS406/SPA2-GFP	This study
RDY247	*MAT***a** *ste4*$^{T320A\ S335A}$ *bud1*Δ::*KAN bar1*Δ *ade1 his2 leu2-3, 112 trp1-1a ura3*Δ pRS406/SPA2-GFP	This study
RDY259	*MAT***a** *bud1*Δ::*KAN bar1*Δ *ade1 his2 leu2-3, 112 trp1-1a ura3*Δ pRS424/GFP-CDC42	This study
RDY260	*MAT***a** *ste4*$^{T320A\ S335A}$ *bud1*Δ::*KAN bar1*Δ *ade1 his2 leu2-3, 112 trp1-1a ura3*Δ pRS424/GFP-CDC42	This study
EAY106	*MAT***a** *bud1*Δ::*KAN bar1*Δ *ade1 his2 leu2-3, 112 trp1-1a ura3*Δ pRS304/STE2$^{7XR/GPAAD}$	This study
EAY107	*MAT***a** *ste4*$^{T320A\ S335A}$ *bud1*Δ::*KAN bar1*Δ *ade1 his2 leu2-3, 112 trp1-1a ura3*Δ pRS304/STE2$^{7XR/GPAAD}$	This study
ODY111	*MAT***a** *bar1*Δ *ade1 his2 leu2-3, 112 trp1-1a ura3*Δ YCplac111/GAL1-Ste4 pESC /GAL10-FLAG-Far1	This study
ODY113	*MATa bar1*Δ *ade1 his2 leu2-3, 112 trp1-1a ura3*Δ YCplac111/GAL1- ste4$^{T320A\ S335A}$ pESC /GAL10-FLAG-Far1	This study
NWY051	*MAT***a** *bar1*Δ *ade1 his2 leu2-3, 112 trp1-1a ura3*Δ *ste18*Δ::*URA3 lys1*Δ::KanMX *arg5*/*arg6*Δ::G418 YCplac111/GAL1- ste4$^{T320A\ S335A}$	This study
NWY052	*MAT***a** *bar1*Δ *ade1 his2 leu2-3, 112 trp1-1a ura3*Δ *ste18*Δ::*URA3 lys1*Δ::KanMX *arg5*/*arg6*Δ::G418 YCplac111/GAL1-Ste4	This study

Strain construction: All strains used in this study were derived from strain 15Dau (*MAT***a** *bar1*D *ade1 his2 leu2-3*, *-112 trp1 ura3*D), which is congenic with strain BF264-15D (Reed et al. 1985). RDY114 was generated by *in situ* transplacement of *ste4*Δ::*URA3* in strain ELY104 (Li et al., 1998b) with $ste4^{T320A\ S335A}$, excised as an *Eco*RI-*Sph*I fragment from the plasmid YCplac33/ $ste4^{T320A\ S335A}$ (Li et al., 1998a). Recombinants were selected on 5′FOA and confirmed by sequencing. The *BUD1/RSR1* locus was deleted in strains 15Dau *bar1*Δ and RDY114 to create strains RDY103 and RDY120, respectively, using a *bud1*Δ*::KANMX4* cassette which was PCR-amplified from pFA6a-Kan (Wach, 1996) using the oligomers 5′- GCGCATTCATCCTCGACATTCTCAAACGCGAAATATCGTCGAACGTACGCTGCAG GTCGACGG - 3′ and 5′- GTTGTGAAGTAGCGCTAATTCCTGTCCTGTTGCTAGAACCAGATA TCGATGAATTCGAGCTCG - 3′. GFP-tagging was performed *in situ* by transplacement of an excised *Eco*RI-*Sma*I fragment from pRS316/*STE4*p-*GFP-STE4* (Kim et al., 2000) or pRS316/*STE4*p-$GFP\text{-}ste4^{T320A\ S335A}$ (RDB122, see construction below) into strain ELY104 to create strains RDY126 and RDY139, respectively. The *BUD1/RSR1* locus was deleted as described above in strains RDY126 and RDY139 to create strains RDY130 and RDY132, respectively. RDY114 was transformed with pGAL-HO and the mating type was switched to generate RDY217 as described (Guthrie and Fink, 2002). Strains EAY106 and EAY107 were created by transforming pRS304/$STE2^{7XR/GPAAD}$ cut with BsmI into strains RDY103 and RDY120, respectively, and confirmed by sequencing.

REFERENCES

Guthrie, C. and Fink, G. R. (2002). Guide to Yeast Genetics and Molecular Biology. San Diego, CA.: Academic Press.

Kim, J., Bortz, E., Zhong, H., Leeuw, T., Leberer, E., Vershon, A. K. and Hirsch, J. P. (2000). Localization and signaling of Gβ subunit Ste4p are controlled by a-Factor receptor and the a-specific protein Asg7p. *Mol. Cell. Biol.* **20**, 8826-8835.

Li, E., Cismowski, M. J. and Stone, D. E. (1998a). Phosphorylation of the pheromone-responsive Gbeta protein of Saccharomyces cerevisiae does not affect its mating-specific signaling function. *Mol Gen Genet* **258**, 608-18.

Li, E., Meldrum, E., Stratton, H. and Stone, D. E. (1998b). Substitutions in the pheromone responsive Gβ protein of Saccharomyces cerevisiae confer a defect in recovery from pheromone treatment. *Genetics* **148**, 947-961.

Reed, S. I., Hadwiger, J. A., and Lorincz, A. T. (1985). Protein kinase activity associated with the product of the yeast cell division cycle gene CDC28. *Proc Natl Acad Sci USA* **82**, 4055-4059.

Wach, A. (1996). PCR-synthesis of marker cassettes with long flanking homology regions for gene disruptions in S. cerevisiae. *Yeast* **12**, 259-265.

Supplementary Table 2. Plasmids used in this study

Plasmid no	Plasmid name	Marker/Type	Source
DSB159	YCplac22/GPA1	TRP1/CEN	(Stratton et al., 1996)
MMB104	YCplac22/gpa1$^{K21E\ R22E}$	TRP1/CEN	(Metodiev et al., 2002)
RDB116	YCplac33/ste4$^{T320A\ S335A}$	URA3/CEN	(Li et al., 1998a)
BLT49	pRS316/GFP-Ste4	URA3/CEN	(Kim et al., 2000)
RDB122	pRS316/GFP- ste4$^{T320A\ S335A}$	URA3/CEN	This study
RDB151	pRS406/Spa2-GFP	URA3/INT	(Arkowitz and Lowe, 1997)
DLB2823	pRS305/Bem1-GFP-Snc2	LEU2/INT	(Howell et al., 2009)
	pRS424/GFP-Cdc42	URA3/2µm	(Barale et al., 2006)
DLB3217	pRS304/STE2$^{7XR/GPAAD}$	TRP1/INT	Lew lab
MCB26	YCplac111/GAL1-Ste4	LEU2/CEN	(Cismowski et al., 2001)
RDB131	YCplac111/GAL1- ste4$^{T320A\ S335A}$	LEU2/CEN	This study
pEB15.1	pESC /GAL10-FLAG-Far1	URA3/2µm	This study

Plasmid construction: The plasmids used in this study are listed in Table S2. RDB122 was created by sequential site-directed mutagenesis of pRS316/*STE4*p-*GFP-STE4*, and YCplac111/GAL1- STE4$^{T320A\ S335A}$ was created by sequential site-directed mutagenesis of YCplac111/GAL1- STE4, using QuikChange II XL kit (Qiagen). The oligomers used to create the T320A mutation were
5′- CGAGGTTATGAAGAACGTACCCCTGCCCCTACTTATATGGCAGC - 3′and
5′- GCTGCCATATAAGTAGGGGCAGGGGTACGTTCTTCATAACCTCG - 3′. The oligomers used to create the sequential S335A mutation were
5′ - GGAGTACAATACCGCGCAAGCGCCACAAACTTTAAAATCAAC -3′ and
5′ - GTTGATTTTAAAGTTTGTGGCGCTTGCGCGGTATTGTACTCC - 3′. To create

pEB15.1 (pESC/GAL10-FLAG-FAR1), *FAR1* was PCR-amplified from strain15Dau genomic DNA and the product was cloned into pESC-URA as a PacI-BglII fragment, thereby placing *FAR1* under *GAL10* promoter control. The priming oligonucleotides were:

5′ - CCTTAATTAAGCGTAGTATAGACGTGGAG - 3′ and

5′ - GAAGATCTTGAAGACACCAACAAGAGTTTCG - 3′.

REFERENCES

Arkowitz, R. A. and Lowe, N. (1997). A small conserved domain in the yeast Spa2p is necessary and sufficient for its polarized localization. *J Cell Biol* **138**, 17-36.

Barale, S., McCusker, D. and Arkowitz, R. A. (2006). Cdc42p GDP/GTP cycling is necessary for efficient cell fusion during yeast mating. *Mol Biol Cell* **17**, 2824-38.

Cismowski, M. J., Metodiev, M. V., Draper, E. M. and Stone, D. E. (2001). Biochemical analysis of yeast Gα mutants that enhance adaptation to pheromone. *Biochem. Biophys. Res. Comm.* **284**, 247-254.

Howell, A. S., Savage, N. S., Johnson, S. A., Bose, I., Wagner, A. W., Zyla, T. R., Nijhout, H. F., Reed, M. C., Goryachev, A. B. and Lew, D. J. (2009). Singularity in polarization: rewiring yeast cells to make two buds. *Cell* **139**, 731-43.

Kim, J., Bortz, E., Zhong, H., Leeuw, T., Leberer, E., Vershon, A. K. and Hirsch, J. P. (2000). Localization and signaling of Gβ subunit Ste4p are controlled by a-Factor receptor and the a-specific protein Asg7p. *Mol. Cell. Biol.* **20**, 8826-8835.

Li, E., Cismowski, M. J. and Stone, D. E. (1998a). Phosphorylation of the pheromone-responsive Gbeta protein of Saccharomyces cerevisiae does not affect its mating-specific signaling function. *Mol Gen Genet* **258**, 608-18.

Metodiev, M. V., Matheos, D., Rose, M. D. and Stone, D. E. (2002). Regulation of MAPK function by direct interaction with the mating-specific Galpha in yeast. *Science* **296**, 1483-6.

Stratton, H. F., Zhou, J., Reed, S. I. and Stone, D. E. (1996). The mating-specific Gα protein of Saccharomyces cerevisiae downregulates the mating signal by a mechanism that is dependent on pheromone and independent of Gβγ sequestration. *Mol. Cell. Biol.* **16**, 6325-6337.